NASA TM-84589

NASA Technical Memorandum 84589

COMPARISON OF ANALYTICAL AND EXPERIMENTAL STEADY- AND UNSTEADY-PRESSURE DISTRIBUTIONS AT MACH NUMBER 0.78 FOR A HIGH-ASPECT-RATIO SUPERCRITICAL WING MODEL WITH OSCILLATING CONTROL SURFACES

WILLIAM E. MCCAIN

JANUARY 1983

National Aeronautics and Space Administration

Langley Research Center
Hampton, Virginia 23665

COMPARISON OF ANALYTICAL AND EXPERIMENTAL STEADY- AND UNSTEADY-PRESSURE DISTRIBUTIONS AT MACH NUMBER 0.78 FOR A HIGH-ASPECT-RATIO SUPERCRITICAL WING MODEL WITH OSCILLATING CONTROL SURFACES

William E. McCain

SUMMARY

The results of a comparative study using the unsteady aerodynamic lifting-surface theory, known as the Doublet Lattice method, and experimental transonic steady- and unsteady-pressure measurements, are presented for a high-aspect-ratio supercritical wing model. Comparisons of pressure distributions due to wing angle of attack and control-surface deflections were made. Because both the steady and unsteady experimental aerodynamics contained viscous and transonic effects (which cannot be predicted by the inviscid linear lifting-surface theory), some discussion of these effects is also included with the discussions of the experimental and theoretical comparisons. The more significant deviations found between experimental and theoretical data (due to changes in angle of attack and control-surface deflections) were in the vicinity of the outboard control surface.

INTRODUCTION

The substantial improvements in aircraft characteristics envisioned for energy-efficient transports can be a direct result of effectively combining active controls with advanced aerodynamic features such as winglets and supercritical airfoils. The design and analysis of such aircraft require the

use of multipurpose computer programs such as ISAC (ref. 1), SYNPAC (ref. 2), DYLOFLEX (refs. 3 and 4), and the aerodynamic energy method (ref. 5), all of which are currently used at the Langley Research Center. The design of active control systems are very sensitive to the quality of the steady and unsteady aerodynamics employed, particularly at transonic conditions. All the computer programs in refs. 1 through 5 incorporate the unsteady aerodynamic lifting-surface theory known as the Doublet Lattice method.

For comparison and validation of unsteady aerodynamic theories, the National Aeronautics and Space Administration (NASA) conducted a series of wind-tunnel tests in the Langley Transonic Dynamics Tunnel (TDT) to provide a comprehensive data base of measured transonic unsteady pressures, using a semispan model of a high-aspect-ratio supercritical wing with oscillating control surfaces. Two wind-tunnel entries provided measured steady and unsteady pressures for two trailing edge control surfaces and one leading edge control surface (refs. 6 and 7). The wind-tunnel test conditions included variations in Mach number, Reynolds number, wing angle of attack, control-surface deflection angle, and control-surface oscillation amplitude and frequency.

This paper compares experimental steady- and unsteady-pressure distributions with calculations using the Doublet Lattice method at a Mach number of 0.78. Similar comparisons have been made at M = 0.60 in ref. 8. (A preliminary comparison has been made at M = 0.78, using the unsteady aerodynamics of a Kernel function method (refs. 9 & 10), in ref. 11). The comparisons of the present paper will assist in the development and verification of empirical correction methods that can be applied to the Doublet Lattice calculations.

SYMBOLS

AR	aspect ratio, b_0^2/S
$b_0/2$	wing semispan, m
b	wing root semichord, m
c	streamwise local chord, m
c_{av}	wing average chord, m
c_ℓ	section lift coefficient
c_m	section pitching-moment coefficient about the leading edge
C_p	pressure coefficient
C_p^*	pressure coefficient at the critical Mach number
C'_p	lifting-surface steady-pressure coefficient, $C_{p_{l.s.}} - C_{p_{u.s.}}$
$\Delta c_\ell/\Delta\alpha$	increment in section lift coefficient per change in angle of attack, deg^{-1}
$\Delta c_\ell/\Delta\delta$	increment in section lift coefficient per change in control-surface deflection, deg^{-1}
$\Delta c_m/\Delta\alpha$	increment in section pitching-moment coefficient about the leading edge per change in angle of attack, deg^{-1}
$\Delta C'_p/\Delta\alpha$	increment in lifting-surface pressure coefficient per change in angle of attack, deg^{-1}
$\Delta C'_p/\Delta\delta$	increment in lifting-surface pressure coefficient per change in control-surface deflection, deg^{-1}

$\lvert C'_p \rvert$	magnitude of lifting-surface unsteady-pressure coefficient
f	frequency of oscillating control surface, Hz
k	reduced frequency, $b\omega/V$
M	free-stream Mach number
q	free-stream dynamic pressure, kPa
R	Reynolds number based on wing average chord
S	total wing planform area, m^2
t/c	thickness-to-chord ratio
V	free-stream velocity, m/sec
x	streamwise coordinate, m
x/c	fraction of local streamwise chord
y	spanwise coordinate, m
z	vertical coordinate, positive up, m
α	wing angle of attack, deg
δ	control-surface deflection angle, positive trailing edge down, deg
$\Delta\alpha$	change in wing angle of attack, deg
$\Delta\delta$	change in control-surface deflection angle, deg
$\Lambda_{l.e.}$	leading-edge sweepback angle, deg
η	fraction of semispan, $2y/b_0$
ϕ	phase angle of unsteady pressure, referenced to control-surface motion (negative for pressure changes lagging the control-surface motion)
ω	circular frequency of oscillating control surface, rad/sec

Subscripts and Abbreviations

C.S.	control surface
l.e.	leading edge
l.s.	lower surface
ref.	reference
u.s.	upper surface

MODELS

Wind-Tunnel Model

A sketch depicting the geometric properties of the wind-tunnel model is presented in figure 1. The wing has an aspect ratio of 10.76, a leading edge sweep-back angle of 28.8°, and a semispan of 2.286 meters. The table in figure 1 lists the designated spanwise stations for each of the nine chordwise sets of static-pressure orifices. The wing has a total of 252 static-pressure orifices and a total of 164 dynamic-pressure transducers at locations closely corresponding to the static-pressure orifices. Both the static-pressure orifices and dynamic-pressure transducers were installed in chordwise opposing sets on the upper and lower surface to facilitate obtaining lifting-pressure distributions. A total of 10 independently oscillating control surfaces were available on the wing, however, only two at the trailing edge, with hinge lines on the 80 percent chord, were considered in this study: an inboard control surface located between 10 and 24 percent semispan and an outboard control surface between 59 and 79 percent semispan (identified as numbers 6 and 9 in refs. 6 and 7).

The cross-sectional shape of the model consists of NASA super-critical-airfoil sections of varying chord length and thickness as shown in figure 2. Further details of the wind-tunnel model, including airfoil shape quality and structural rigidity are described in refs. 6, 7, and 12.

Analytical Model

An aerodynamic model was generated for use in the subsonic unsteady lifting-surface theory known as the Doublet Lattice method (ref. 13). The arrangement of aerodynamic boxes representing the wind-tunnel model is shown in figure 3. To provide more calculated pressure points for comparative purposes, the chordwise and spanwise distributions of aerodynamic boxes were increased over the planform areas near and on the control surfaces. The aerodynamic boxes in figure 3 with asterisks identify the control surfaces and the cross-hatched strips identify the locations corresponding to the nine semispan stations shown in figure 1. There were 42 streamwise strips, a total of 325 aerodynamic boxes, used to comprise the model layout. In creating this box layout, an attempt was made to keep the aspect ratio of each box as close to 1.0 as possible.

EXPERIMENTAL DATA

All the experimental data presented herein were obtained at the test conditions of $M = 0.78$, $R = 2.2 \times 10^6$ (based on the wing average chord), and $q = 3.9$ kPa.

Steady-Pressure Data

A summary of the conditions at which the steady-pressure data were taken is presented in Table I. All the steady-pressure data for this study are presented in ref. 6, which identifies each data set by the test point numbers also listed in Table I for convenience. The test conditions included angles of attack ranging from -3° to 4°, and control surface deflection angles ranging

from -6° to 6°. The steady-pressure data for both inboard and outboard control surface deflections were obtained at a 2.05° angle of attack.

The experimental data from ref. 6 consisted of tabulated steady-pressure coefficients, C_p, on both upper and lower surfaces of the wing with the corresponding lifting-surface steady-pressure coefficients, $C_p' = C_{p_{l.s.}} - C_{p_{u.s.}}$. The section lift coefficient, c_ℓ, and section pitching-moment coefficient about the leading edge, c_m, at each of the nine spanwise stations were obtained by numerically integrating equations (1) and (2), respectively.

$$c_\ell = \frac{1}{c}\int_0^1 C_p' \, dx \tag{1}$$

$$c_m = \frac{1}{c^2}\int_0^1 C_p' \, x \, dx \tag{2}$$

Calculations were also made for the incremental changes in those coefficients due to angle of attack or control-surface deflection changes, as follows:

$$\frac{\Delta c_\ell}{\Delta \alpha} = \frac{c_\ell - c_{\ell_{ref}}}{\alpha - \alpha_{ref}} \tag{3}$$

$$\frac{\Delta C_{\ell}}{\Delta \delta} = \frac{C_{\ell} - C_{\ell_{ref}}}{\delta - \delta_{ref}} \tag{4}$$

$$\frac{\Delta C_m}{\Delta \alpha} = \frac{C_m - C_{m_{ref}}}{\alpha - \alpha_{ref}} \tag{5}$$

$$\frac{\Delta C_p'}{\Delta \alpha} = \frac{C_p' - C_{p_{ref}}'}{\alpha - \alpha_{ref}} \tag{6}$$

$$\frac{\Delta C_p'}{\Delta \delta} = \frac{C_p' - C_{p_{ref}}'}{\delta - \delta_{ref}} \tag{7}$$

The reference quantities correspond to the zero-valued test conditions (α_{ref} = 0° and δ_{ref} = 0°).

The status of the experimental steady-pressure data is presented in Table II. C_p' data were unavailable at only a few orifice locations for certain test points as noted in Table II. Some C_p' data were considered unusable due to their abnormal excursions from trends observed at similar test conditions. The available C_p' data was enhanced by the geometric curve-fit method of ref. 14 to provide a well defined chordwise distribution before being numerically integrated by a cubic spline routine.

Unsteady-Pressure Data

A summary of the conditions at which the unsteady-pressure data were taken is presented in Table III. Again, the test point numbers identify the data as obtained from ref. 6 or 7. Each control surface was oscillated about a zero

mean deflection angle with an amplitude of ±6° for three frequencies of oscillation (5, 10, 15 Hz). Depending on the exact tunnel speed for a given test point, the corresponding reduced frequencies varied slightly about the average values of 0.105, 0.210, and 0.315, respectively. Test conditions also included two angles of attack, 0° and 2.05°. The unsteady-pressure measurements are presented in the form of the magnitude of the lifting-surface unsteady-pressure coefficient, $|C_p'|$, and phase angle, ϕ. All phase angles were referenced to the control-surface motion, with negative values for pressure changes lagging the control-surface motion. Although unsteady-pressure measurements were made at all nine semispan stations, only the chordwise distributions at two locations (one near the center of each control surface; rows 1 and 6 in figure 1) were considered in this study.

The status of the experimental unsteady-pressure data is presented in Table IV. To provide thorough chordwise unsteady-pressure distributions at the two semispan stations presented, corresponding results from both wind-tunnel entries (refs. 6 and 7) were used. Data available from ref. 7 provided the most measurements aft of the hinge line at both of the two semispan stations. Again, as previously discussed for the steady data, there were a few data points considered unusable.

ANALYSIS

The Doublet Lattice formulation solves the linearized acceleration or pressure potential-flow equations on zero thickness lifting surfaces at subsonic speeds with nonplanar boundary conditions. The Doublet Lattice method (ref. 13) was used to generate the theoretical steady and unsteady aerodynamics herein. The calculations were performed by the version of the Doublet Lattice program

which is used in a NASA computer program system known as ISAC (Interaction of Structures, Aerodynamics, and Controls, ref. 1). The results of ref. 12 indicated that the wind-tunnel model was essentially rigid and that pressure-measurement results were not significantly influenced by model flexibility. Therefore, only four rigid body modes (plunge, pitch, inboard, and outboard control-surface deflections) of the model were included in the analysis at a Mach number of 0.78. The average reduced frequency values of 0, 0.105, 0.210, and 0.315 were used in the analysis, corresponding to those at which experimental data were available in refs. 6 and 7.

For each mode and at each reduced frequency, the output from the Doublet Lattice program consists of complex lifting-surface pressure coefficients on each aerodynamic box. Since the program performs the necessary numerical integrations internally, the complex section lift and moment coefficients are also listed. At zero reduced frequency (steady), the imaginary parts of these complex quantities are zero. The real and imaginary parts of the unsteady quantities were converted to magnitudes and phase angles for direct comparison to the experimental values from refs. 6 and 7.

COMPARISON OF ANALYSIS AND EXPERIMENT

Steady-Pressure Results

A typical comparison of incremental lifting-surface pressure distribution for each of the incremental angles of attack is shown at semispan station η = 0.51 in figure 4. The "bulge" in the experimental chordwise steady-pressure distributions forward of the midchord (from x/c = 0.1 to x/c = 0.5) and the significant magnitudes in experimental scatter can be attributed to transonic effects. The bulge in pressure is due to the compression, or shock, regions in the steady flow, which move with each change in angle of attack (ref. 15).

Note that the experimental scatter at each chordwise location varies nonlinearly with each incremental angle of attack.

Further comparisons at all nine semispan stations are shown in figures 5(a) through 5(i) for average values of incremental lifting-surface pressure distributions per incremental angle of attack with vertical lines through each symbol to indicate the experimental scatter. The Doublet Lattice data underpredict the average chordwise steady-pressure distributions foward of the midchord and overpredict values aft of the midchord. As discussed in ref. 9, this general trend in deviation between experimental and theoretical data is typical of airfoil thickness (viscosity) effects.

The movement of critical flow regions (local pressure coefficients exceed the critical pressure coefficient, C_p^*) influences the experimental scatter in chordwise steady-pressure distributions. Figure 6 illustrates the critical flow regions at semispan station $\eta = 0.51$ for three angles of attack. Usually the chordwise steady-pressure distribution forward of an aft critical point is characterized by critical flow. Therefore, the movement of critical flow regions with changes in angle of attack can be qualitatively observed by the chordwise movement of aft critical points, as shown in figure 6. Figure 7 depicts the effect of angle of attack on aft critical point locations at each semispan station. The nonlinear movement of the aft critical points shown in figure 7 especially for the outboard half of the wing can be regarded as an indication of the sensitivity of the critical flow region to changes in angle of attack. Obviously, the magnitude in experimental scatter of the chordwise steady-pressure distribution is directly influenced by the sensitivity of the critical flow regions to angle of attack.

The integrated results of the local incremental lifting-surface pressure distributions for section lift and pitching-moment coefficients are compared

with Doublet Lattice results in figures 8(a) and 8(b). The experimental average values of the section lift and pitching-moment coefficients are consistently underpredicted by the Doublet Lattice program. Although the integration is a smoothing process, there is still considerable experimental scatter, especially at the outboard semispan stations. Figure 9 presents the spanwise distribution of local aerodynamic center locations. The experimental average values of local aerodynamic center locations closely match the Doublet Lattice calculations. This result can be misleading since the aerodynamic center values are based on the ratio of the section pitching-moment coefficients to section lift coefficients, both of which are underpredicted by the Doublet Lattice program.

The incremental lifting-surface pressure distributions for incremental control-surface deflections are shown in figures 10 and 11. Figure 10 presents comparisons for the inboard control-surface data at semispan station $\eta = 0.19$; figure 11 presents comparisons for the outboard control surface data at semispan station $\eta = 0.71$. The comparisons are at 2.05° angle of attack for three positive and negative incremental control-surface deflection angles ($\Delta\delta = \pm 2°, \pm 4°, \pm 6°$). In comparing the Doublet Lattice and experimental pressure distributions, there are two discrepancies which indicate the presence of transonic effects in the experimental data (ref. 15): (1) near the leading edge (forward of the 20 percent chord), the reduced magnitude of experimental pressures compared to analytical pressures; and (2) near the midchord, the bulge in the experimental pressures compared to analytical pressures. The experimental outboard control surface results show considerably more sensitivity to transonic effects. Note the large excursions between the experimental outboard control-surface data for positive and negative deflection angles, shown in figure 11, compared to the smoother trends shown in figure 10, for the

experimental inboard control-surface data. The experimental outboard control-surface data exhibited possible separated flow toward the trailing edge of the deflected control surface. For positive outboard control-surface deflections, there was a rise in the steady-pressure distribution at the 95 percent chord location after a drop in pressure at the 90 percent chord location. In general, these are the most significant deviations between experimental and theoretical comparisons, along with the Doublet Lattice overprediction of experimental pressures aft of the control-surface hinge lines ($x/c = 0.80$).

Figure 12 presents the chordwise movement of aft critical points at the inboard and outboard semispan stations due to control surface deflections. The outboard aft critical points move more rapidly toward the control surface hinge line than the inboard aft critical points. This may be an indication of the greater sensitivity of the experimental outboard control surface results to transonic effects (compared to inboard control surface results), previously discussed.

The incremental section lift coefficient distributions for both inboard and outboard incremental control-surface deflections are shown in figures 13(a) and 13(b), respectively. The average experimental values are taken over the six incremental control-surface deflections presented in figures 10 and 11. The experimental scatter is again indicated by vertical lines through each symbol. The experimental averages for both sets of control-surface data deviate noticeably from the Doublet Lattice calculations at the outboard semispan stations. The analytical results for the inboard control-surface data consistently underpredict the experimental averages outboard from the inboard control surface. The analytical results for the outboard control-surface data overpredict the experimental averages on the outboard control surface.

Unsteady-Pressure Results

Comparisons of the chordwise unsteady-pressure distributions in the form of magnitude and phase angle are presented in figures 14 and 15. Figure 14 contains comparisons at η = 0.18 (near the center of the inboard control surface) for the inboard surface oscillating at all three frequencies. Figure 15 contains comparisons at η = 0.71 (near the center of the outboard control surface) for the outboard surface oscillating at all three frequencies. The amplitude of both oscillating control surfaces was $\delta = \pm 6°$. The experimental data for both angles of attack (0° and 2.05°) are presented for the two separate test entries (open symbols for ref. 6 data and solid symbols for ref. 7 data). Similar to the steady-pressure comparisons, the Doublet Lattice program overpredicted the experimental unsteady-pressure magnitudes toward the leading edge and aft of the control-surface hinge line. The bulge in pressure near the midchord due to transonic effects was also apparent. The two trailing edge (x/c = 0.90, 0.95) experimental unsteady-pressure measurements exhibited the same separated flow effect on the outboard control surface, as previously shown for the steady-pressure data. The experimental chordwise unsteady-pressure magnitudes and phase angles for the outboard control surface show considerable experimental scatter between the two angles of attack. For the inboard control surface, the Doublet Lattice phase angles, are consistently more negative than the experimental values. This comparison in phase angles is notably better for the inboard surface than for the outboard surface, possibly due to variable transonic effects. There is a noticeable deviation between the theoretical and experimental phase angles at the same trailing edge locations of the outboard control surface which have shown possible separated flow effects in the pressure magnitude data.

CONCLUDING REMARKS

This paper presents comparisons of theoretical and experimental steady- and unsteady-pressure distributions on a high-aspect-ratio supercritical wing model at a Mach number of 0.78. The theoretical calculations were performed using the unsteady aerodynamic lifting-surface method of Doublet Lattice. Both the steady and unsteady experimental aerodynamics show considerable deviations from calculated values due to viscous and transonic effects, that are not accounted for in the present analysis. Comparisons for the steady data include: chordwise incremental lifting-surface pressure distributions per incremental angle of attack; spanwise incremental lift distributions per incremental inboard and outboard control-surface deflections. Comparisons of theoretical and experimental lifting-surface unsteady-pressure coefficient magnitude and phase angle are shown for both inboard and outboard oscillating control surfaces.

The following observations highlight the more significant differences between the experimental and Doublet Lattice results:

1. For the steady aerodynamics due to incremental angles of attack;
   (a) The Doublet Lattice program underpredicts the experimental chordwise steady-pressure distributions forward of the midchord and overpredicts values aft of the midchord (typical of viscous effects).
   (b) Transonic effects in the experimental chordwise steady-pressure distributions are evident by the bulge forward of the midchord and by the magnitude of scatter throughout the range of incremental angles of attack.
   (c) The Doublet Lattice program underpredicts the experimental spanwise lift and moment distributions.

2. For the steady aerodynamics due to incremental control-surface deflections;

   (a) In general, the Doublet Lattice program overpredicts the experimental chordwise steady-pressure distributions forward of the 20 percent chord and aft of the 80 percent chord.

   (b) There is evidence of flow separation at the trailing edge of the outboard control surface due to positive deflections.

   (c) The maximum deviations between the Doublet Lattice spanwise lift distribution and the experimental average values, due to incremental outboard control-surface deflections, occur within the extent of the outboard control surface.

   (d) The experimental average values of spanwise lift distribution, due to incremental inboard control-surface deflections, depart significantly from the Doublet Lattice results over the semispan stations outboard of the inboard control surface.

3. For the unsteady aerodynamics due to oscillating control surfaces;

   (a) In general, the Doublet Lattice program overpredicts the experimental chordwise unsteady-pressure magnitudes forward of the 20 percent chord and aft of the 80 percent chord.

   (b) There is evidence of flow separation at the trailing edge of the oscillating outboard control surface.

   (c) The Doublet Lattice phase angles, due to the oscillating inboard control surface, are consistently more negative than the experimental values at the leading edge of the inboard semispan station.

REFERENCES

1. Peele, Ellwood, L.; and Adams, William M., Jr.: A Digital Program for Calculating the Interaction Between Flexible Structures, Unsteady Aerodynamics and Active Controls. NASA TM 80040, 1979.

2. Adams, William M., Jr.; and Tiffany, Sherwood H.: Control Law Design to Meet Constraints Using SYNPAC--Synthesis Package for Active Controls. NASA TM 83264, 1982.

3. Miller, R. D.; Kroll, R. I.; and Clemmons, R. E.: Dynamic Loads Analysis System (DYLOFLEX) Summary. NASA CR-2846, 1979.

4. Perry, B., III; Kroll, R. I.; Miller, R. D.; and Goetz, R. C.: DYLOFLEX--A Computer Program for Flexible Aircraft Flight Dynamic Loads Analyses with Active Controls. J. of Aircraft, Vol. 17, April 1980, pp. 275-282.

5. Nissim, E.; and Abel, I.: Development and Application of an Optimization Procedure for Flutter Suppression Using the Aerodynamic Energy Concept. NASA TP 1137, 1978.

6. Sandford, Maynard C.; Ricketts, Rodney H.; and Cazier, F. W., Jr.: Transonic Steady- and Unsteady-Pressure Measurements on a High-Aspect-Ratio Supercritical-Wing Model with Oscillating Control Surfaces. NASA TM 81888, 1980.

7. Sandford, Maynard C.; Ricketts, Rodney H.; and Watson, Judith J.: Subsonic and Transonic Pressure Measurements on a High-Aspect-Ratio Supercritical-Wing Model with Oscillating Control Surfaces. NASA TM 83201, 1981.

8. McCain, William E.: Comparison of Analytical and Experimental Subsonic Steady- and Unsteady-Pressure Distributions for a High-Aspect-Ratio Supercritical Wing Model with Oscillating Control Surfaces. NASA TM 84490, 1982.

9. Rowe, W. S.; Redman, M. C.; Ehlers, F. E.; and Sebastian, J. D.: Prediction of Unsteady Aerodynamic Loadings Caused by Leading Edge and Trailing Edge Control Surface Motions in Subsonic Compressible Flow--Analysis and Results. NASA CR-2543, 1975.

10. Rowe, W. S.; Sebastian, J. D.; and Petrarca, Jr. R.: Reduction of Computer Usage Costs in Predicting Unsteady Aerodynamic Loadings Caused by Control Surface Motions--Analysis and Results. NASA CR-3009, 1979.

11. Sandford, M. C.; Ricketts, R. H.; Cazier, F. W., Jr.; and Cunningham, H. J.: Transonic Unsteady Airloads on an Energy Efficient Transport Wing with Oscillating Control Surfaces. J. of Aircraft, Vol. 18, July 1981, pp. 557-561.

12. Watson, Judith J.: Elastic Deformation Effects on Aerodynamic Characteristics for a High-Aspect-Ratio Supercritical-Wing Model. NASA TM 83286, 1982.

13. Giesing, J. P.; Kalman, T. P.; and Rodden, W. P.: Subsonic Unsteady Aerodynamics for General Configurations, Part I. Direct Application of the Nonplanar Doublet Lattice Method. AFFDL-TR-71-5, Vol. I, November 1971.

14. Akima, Horoshi: A New Method of Interpolation and Smooth Curve Fitting Based on Local Procedures. J. of the Association for Computing Machinery, Vol. 17, No. 4, October 1970, pp. 589-602.

15. Giesing, J. P.; Kalman, T. P.; and Rodden, W. P.: Correction Factor Techniques for Improving Aerodynamic Prediction Methods. NASA CR-144967, 1976.

TABLE I. - SUMMARY OF EXPERIMENTAL STEADY-PRESSURE

TEST CONDITIONS AT M = 0.78

Test Point No.	α	δ
(See Ref. 6)	deg	deg
Angle of Attack		
198	0	0
200	4	|
201	3	|
199	2.58	|
202	2	|
203	1	|
205	-1	|
206	-2	|
207	-3	|
Inboard Control Surface		
409	2.05	0
413	|	6
414	|	4
415	|	2
416	|	0
417	|	-2
418	|	-4
419	|	-6
Outboard Control Surface		
420	2.05	0
422	|	6
423	|	4
425	|	2
426	|	0
429	|	-2
430	|	-4
431	|	-6

TABLE II. - STATUS OF EXPERIMENTAL STEADY-PRESSURE DATA

η \ x/c	.01	.03	.05	.07	.12	.20	.30	.35	.45	.50	.60	.70	.75	.85	.90	.95
.19		(1)												(1)	(2)	
.23	(*)	(*)		(*)												
.25	(*)	(*)		(*)												(3)
.33	(*)	(*)		(*)						(1)						
.51																
.71														(1)		
.78	(*)	(*)		(*)										(1)	(3)	(1)
.81	(*)	(*)		(*)												
.92															(3)	(1)

(*)No orifices installed at these locations.
(1)C'_p unavailable at these locations for all test points in Table I.
(2)C'_p unavailable at this location for test point nos. 198 to 207.
(3)C'_p considered ususable at these locations for test point nos. 409, 419, 429, and 431.

TABLE III. SUMMARY OF EXPERIMENTAL UNSTEADY-PRESSURE TEST CONDITIONS AT M = 0.78

Test Point No.		α	δ	f	k	
Ref. 6	Ref.7	deg	deg	Hz	Ref. 6	Ref. 7
Inboard Control Surface						
271	16	0	±6	5	0.105	0.105
272	17	|	|	10	0.210	0.210
273	18	|	|	15	0.313	0.316
310	37	2.05	|	5	0.105	0.106
311	38	|	|	10	0.210	0.212
312	39	|	|	15	0.315	0.317
Outboard Control Surface						
375	21	0	±6	5	0.105	0.105
377	22	|	|	10	0.208	0.209
378	23	|	|	15	0.313	0.316
343	24	2.05	|	5	0.105	0.105
344	25	|	|	10	0.210	0.209
345	-	|	|	15	0.314	-

TABLE IV. - STATUS OF EXPERIMENTAL UNSTEADY-PRESSURE DATA

η \ x/c	.05	.12	.20	.30	.35	.45	.50	.60	.70	.75	.85	.90	.95
.18		(4)									(1) (3) (4)	(1)	
.71									(2)		(1)	(1)	(1)

(1) $|C'_p|$ and ϕ unavailable at these locations for the ref. 6 points in Table III.

(2) $|C'_p|$ and ϕ unavailable at this location for the ref. 7 test points in Table III.

(3) $|C'_p|$ and ϕ considered unusable at this location for the ref. 7 test point nos. 16, 17, & 18.

(4) $|C'_p|$ and ϕ considered unusable at these locations for the ref. 7 test point nos. 37, 38, & 39.

Orifice Semispan Stations	
Row No.	η
1	0.19
2	0.23
3	0.25
4	0.33
5	0.51
6	0.71
7	0.78
8	0.81
9	0.92

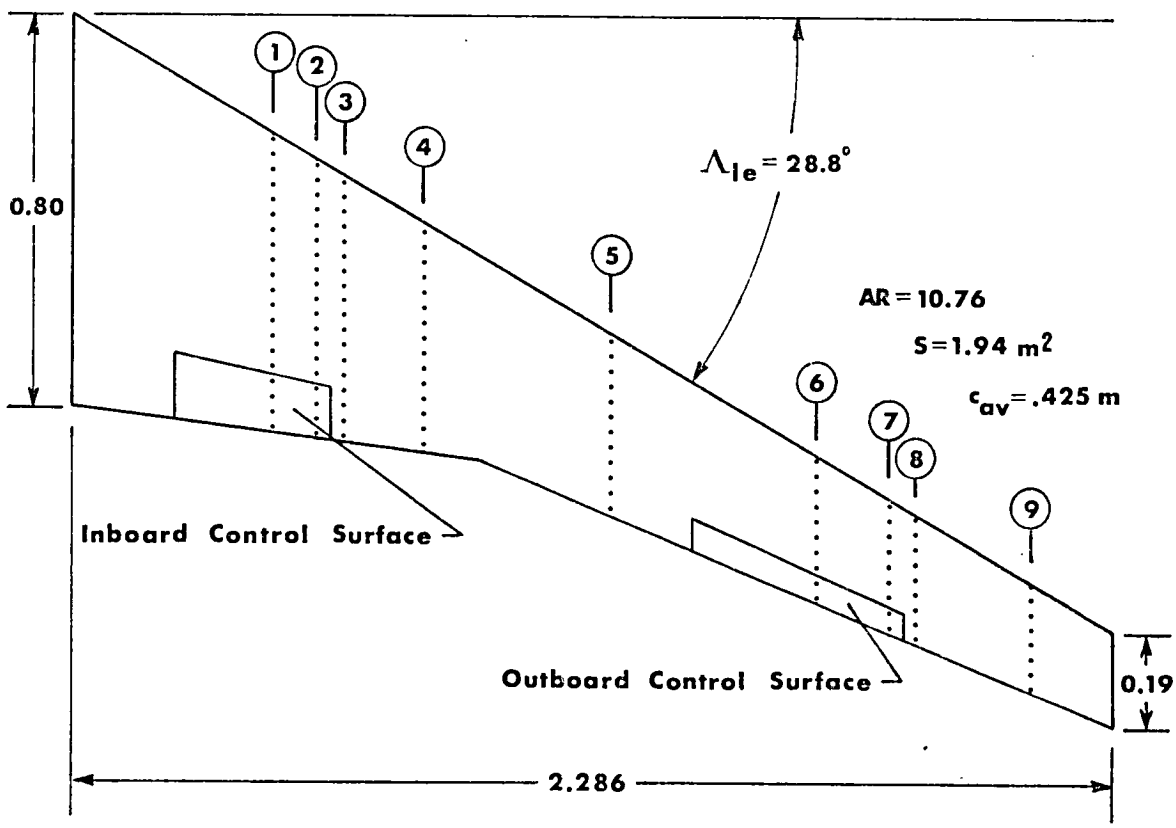

Figure 1. - Sketch of wing planform geometry and orifice semispan stations. Linear dimensions in meters.

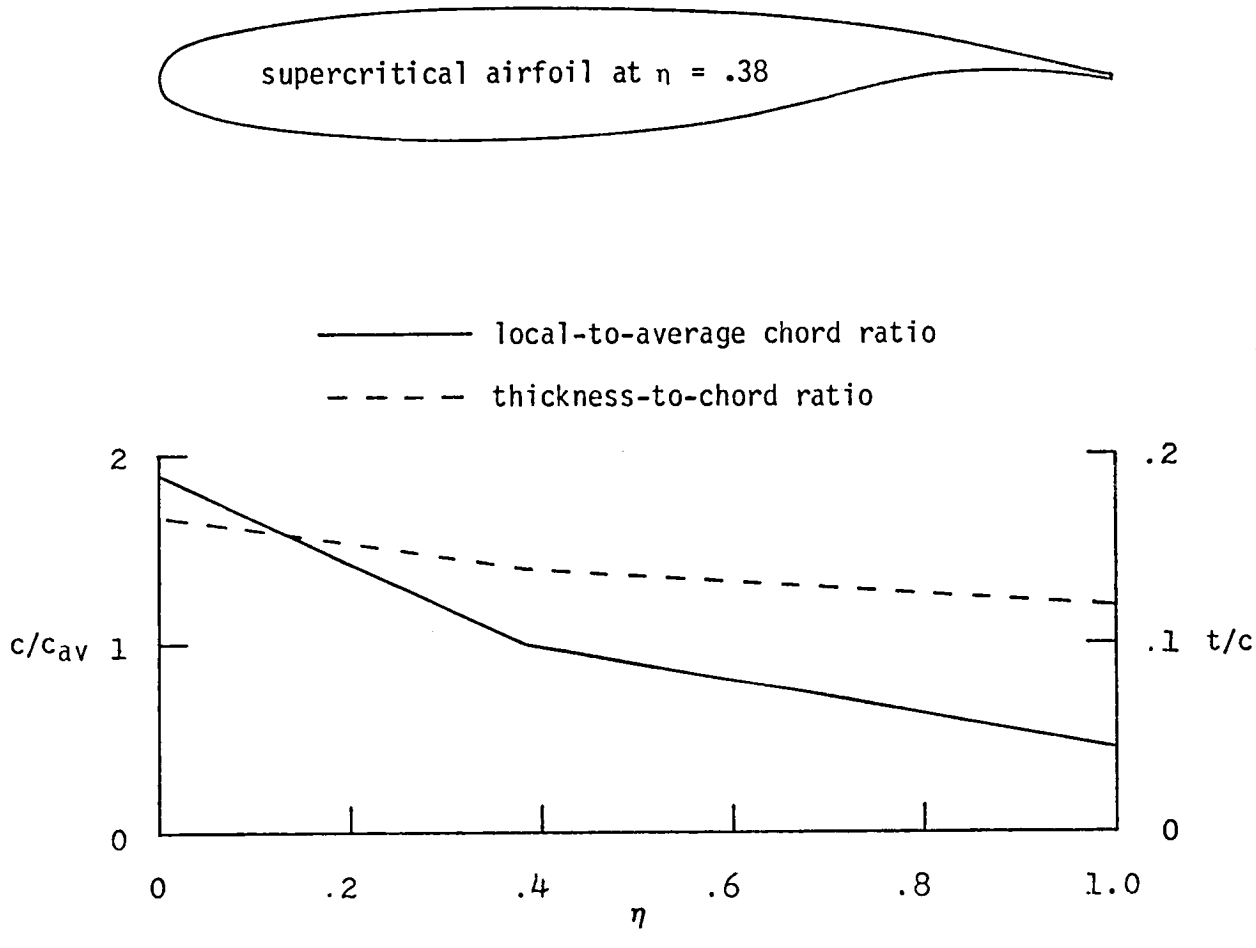

Figure 2.- Sketch of supercritical airfoil for 3-dimensional wind-tunnel model and plot of local chord and thickness variation along semispan.

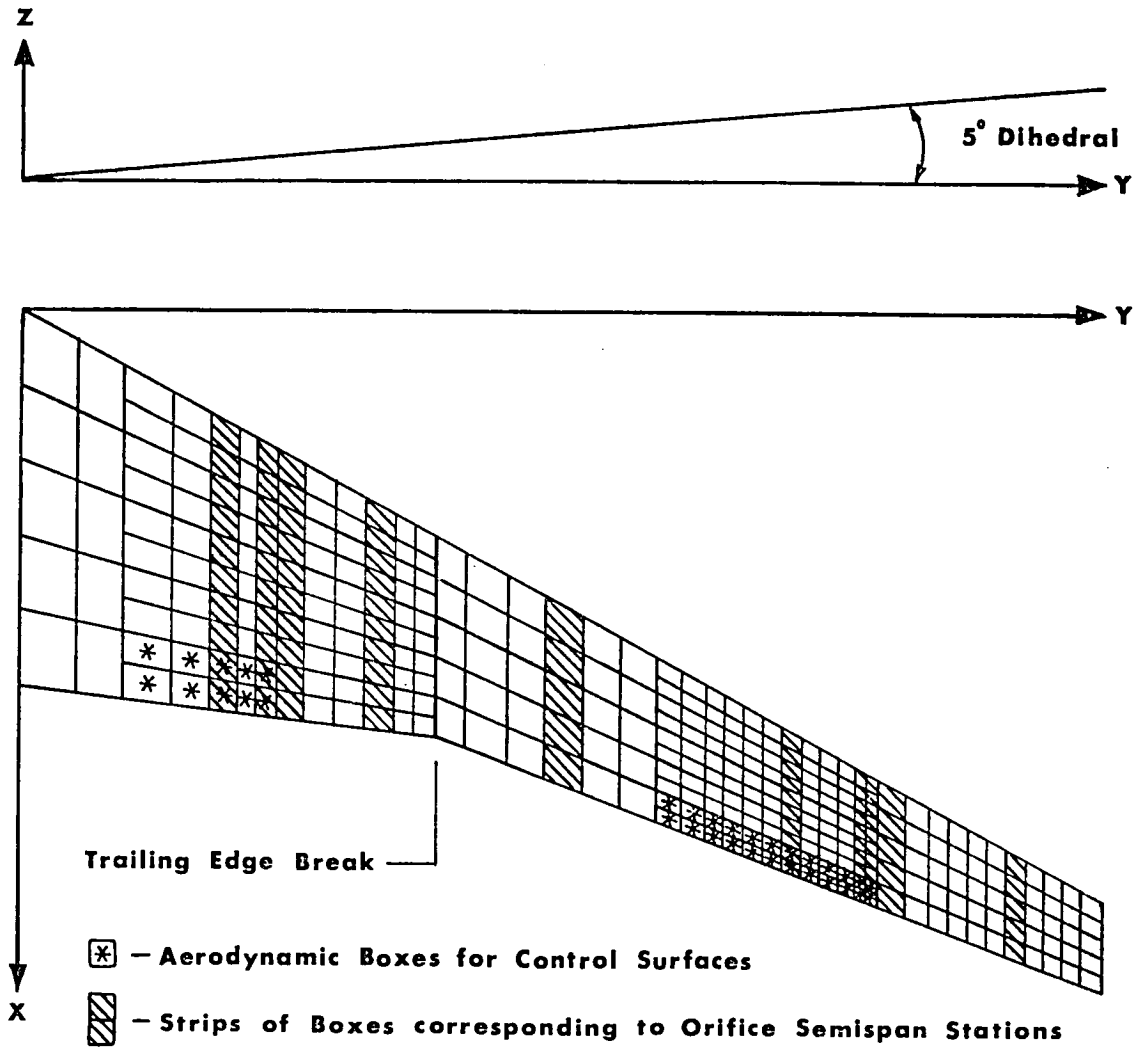

Figure 3.- Sketch of Doublet Lattice aerodynamic model.

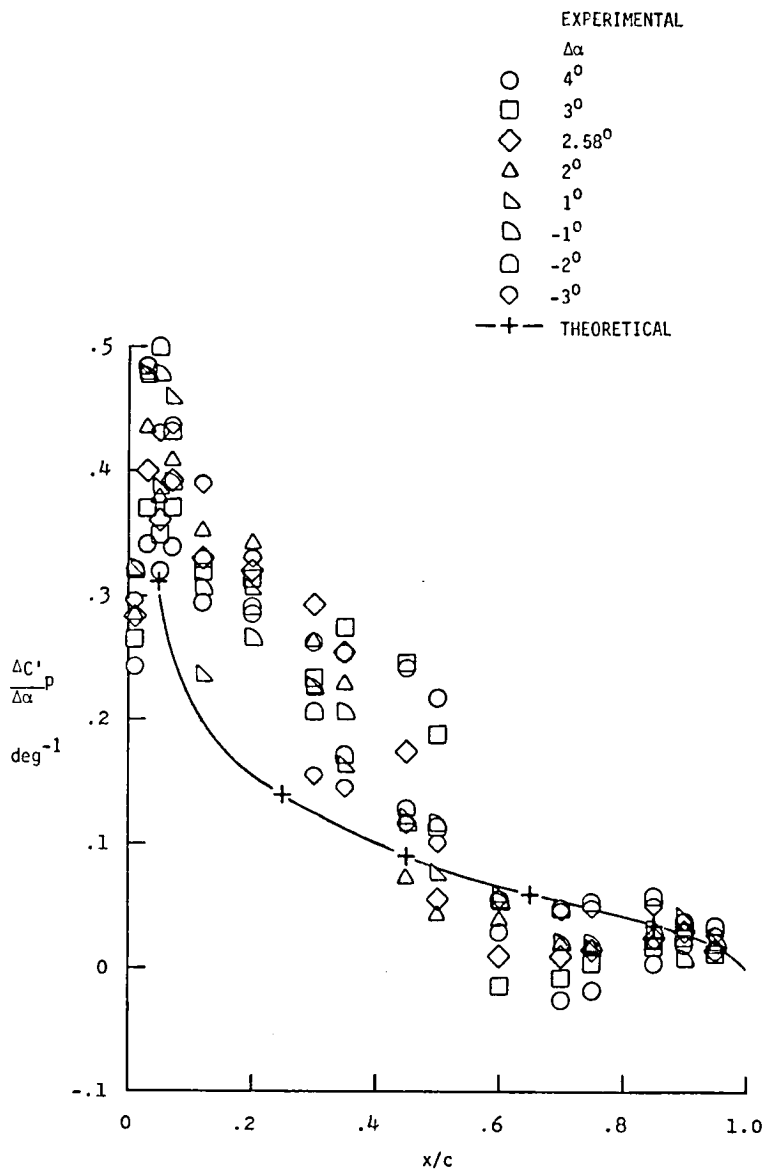

Figure 4. - Chordwise incremental lifting-surface steady-pressure distribution per incremental angle of attack at semispan station $\eta = 0.51$.

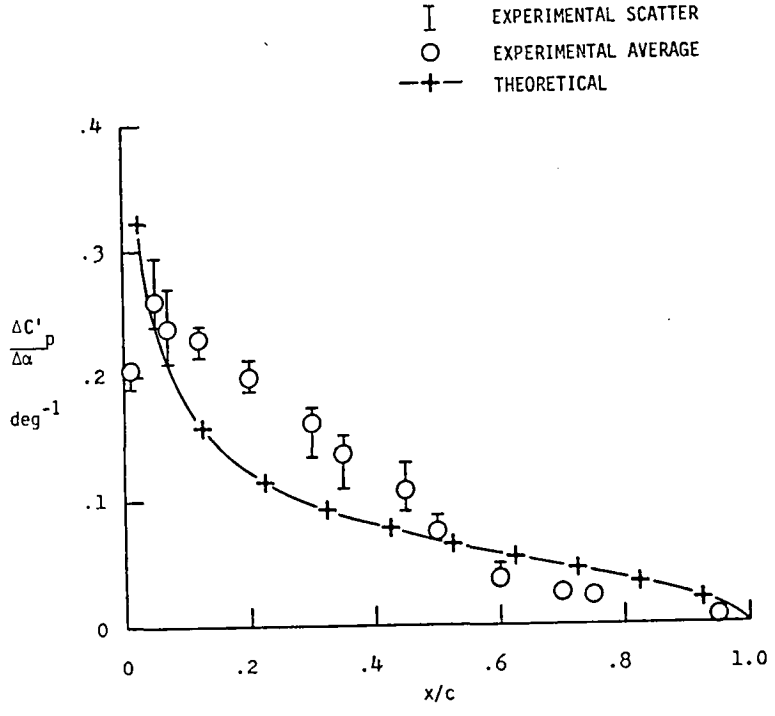

(a) $\eta = 0.19$

Figure 5. - Chordwise incremental lifting-surface steady-pressure distribution per incremental angle of attack.

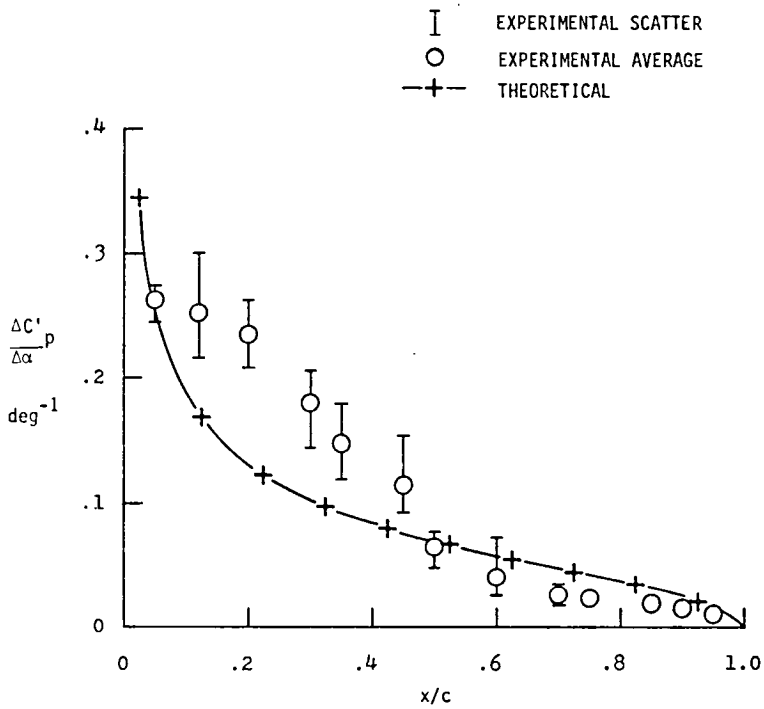

(b) $\eta = 0.23$

Figure 5. - Continued.

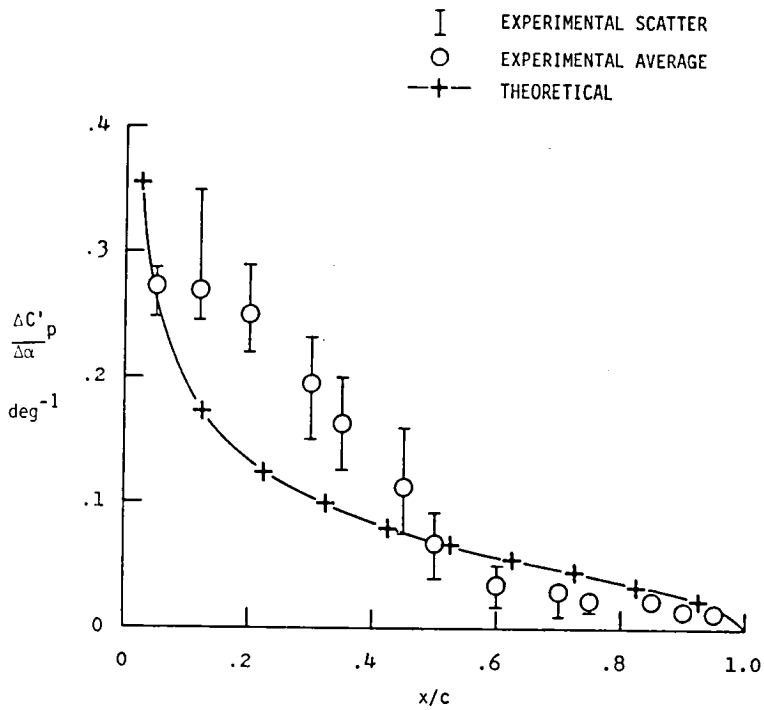

(c) $\eta = 0.25$

Figure 5. - Continued.

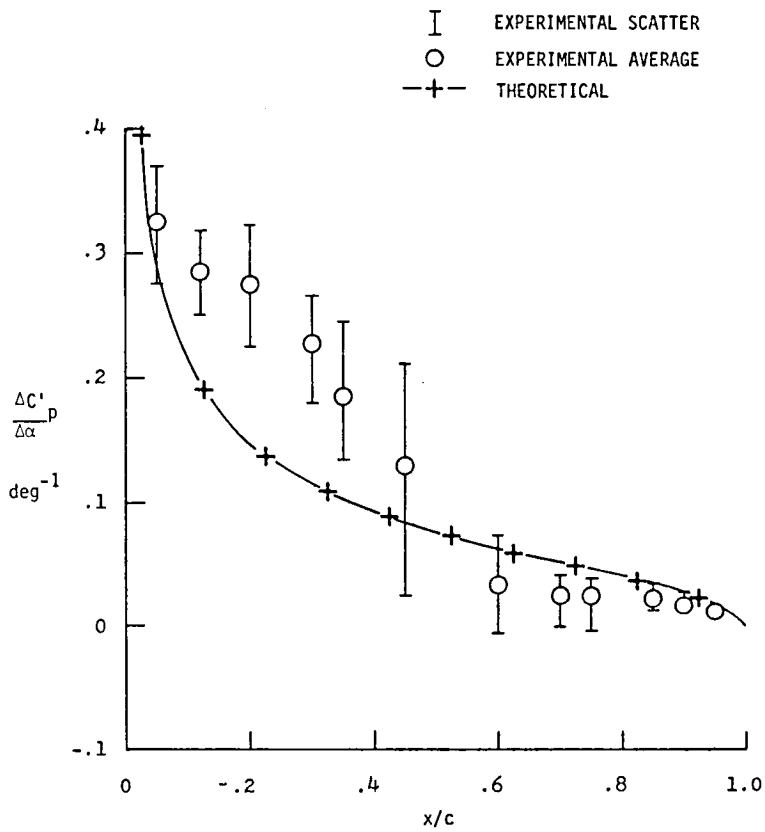

(d) $\eta = 0.33$

Figure 5. - Continued.

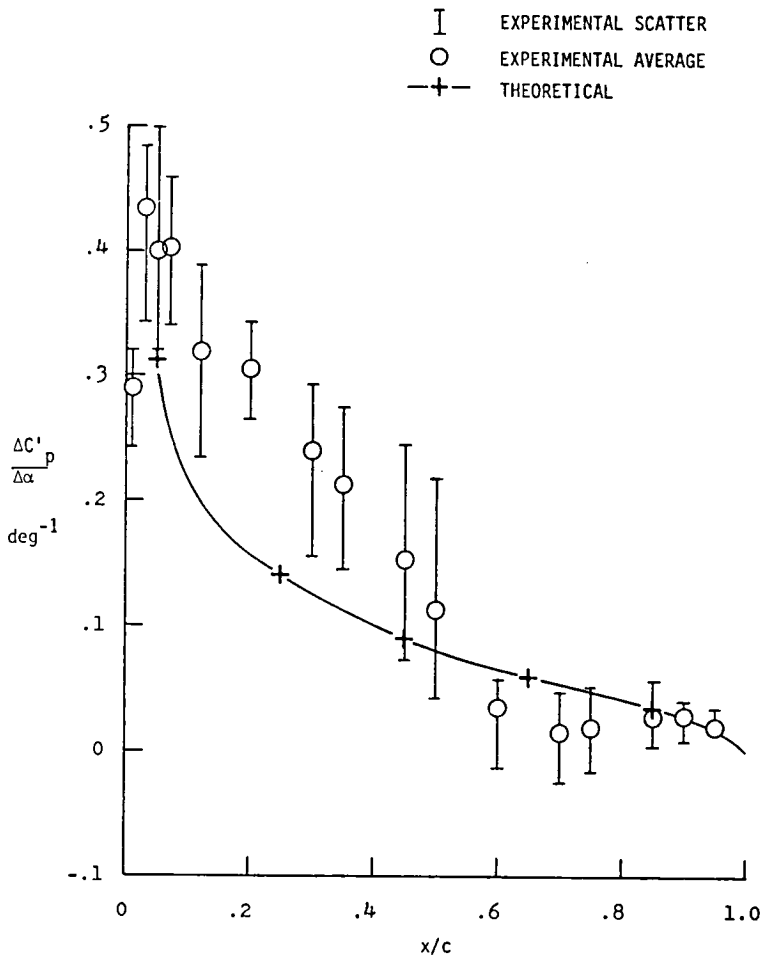

(e) $\eta = 0.51$

Figure 5. - Continued.

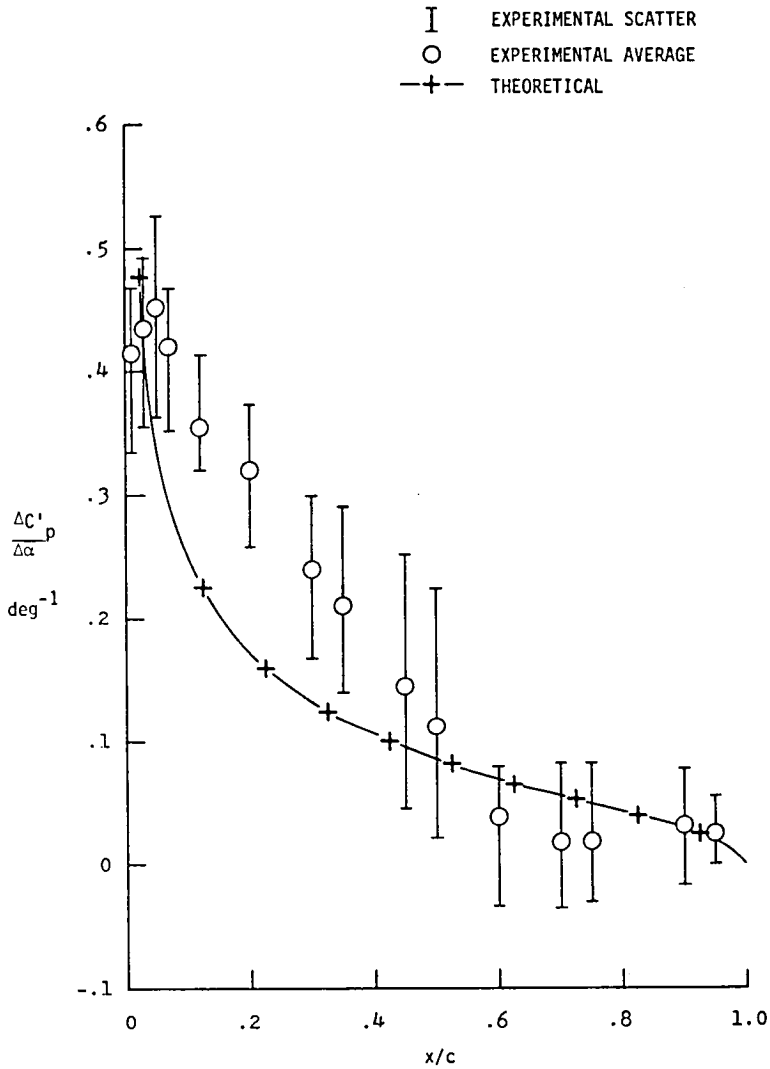

(f) $\eta = 0.71$

Figure 5. - Continued.

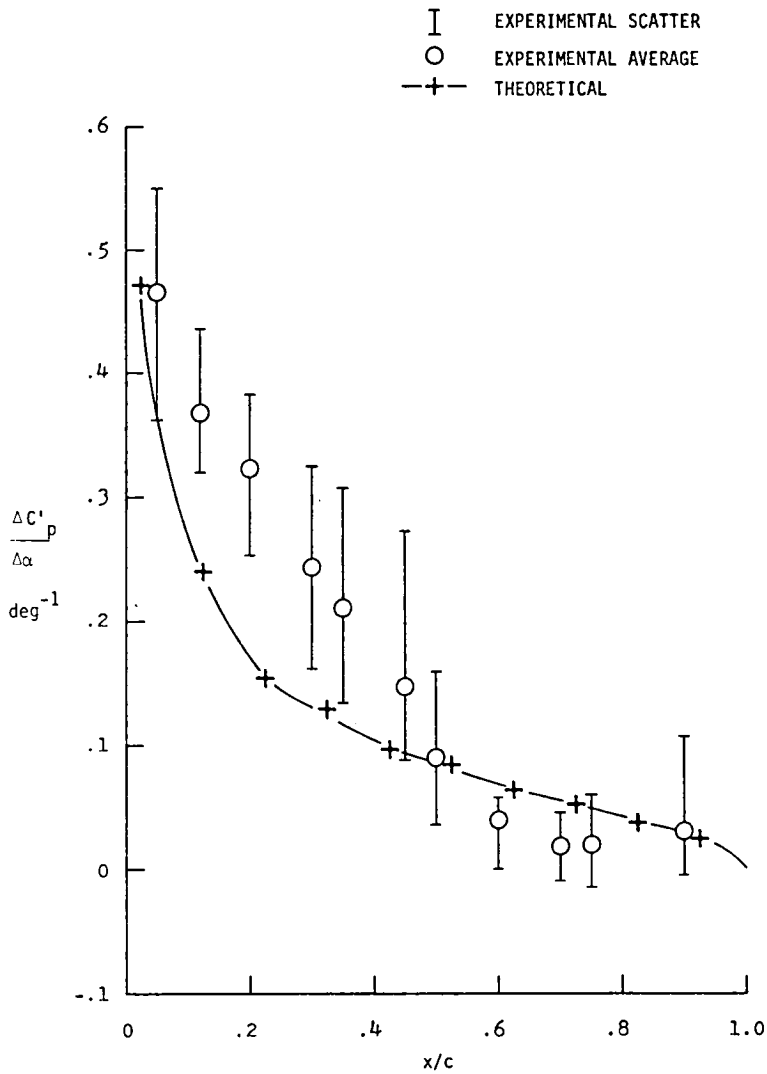

(g) $\eta = 0.78$

Figure 5. - Continued.

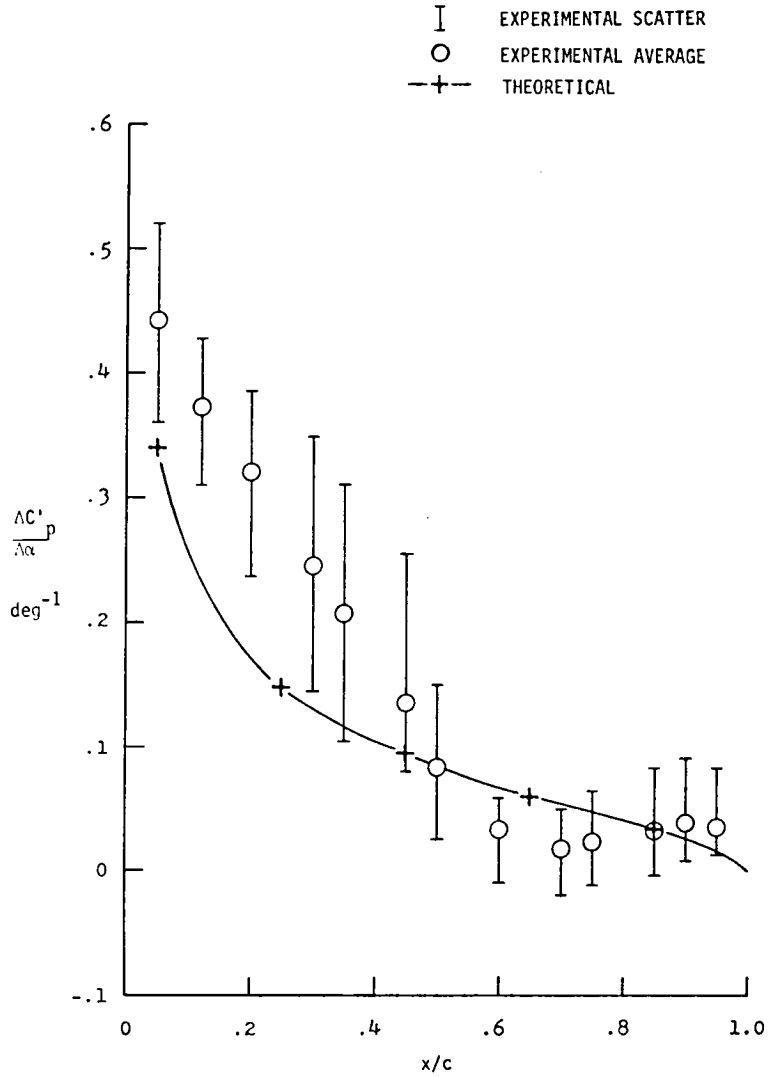

(h) η = 0.81

Figure 5. - Continued.

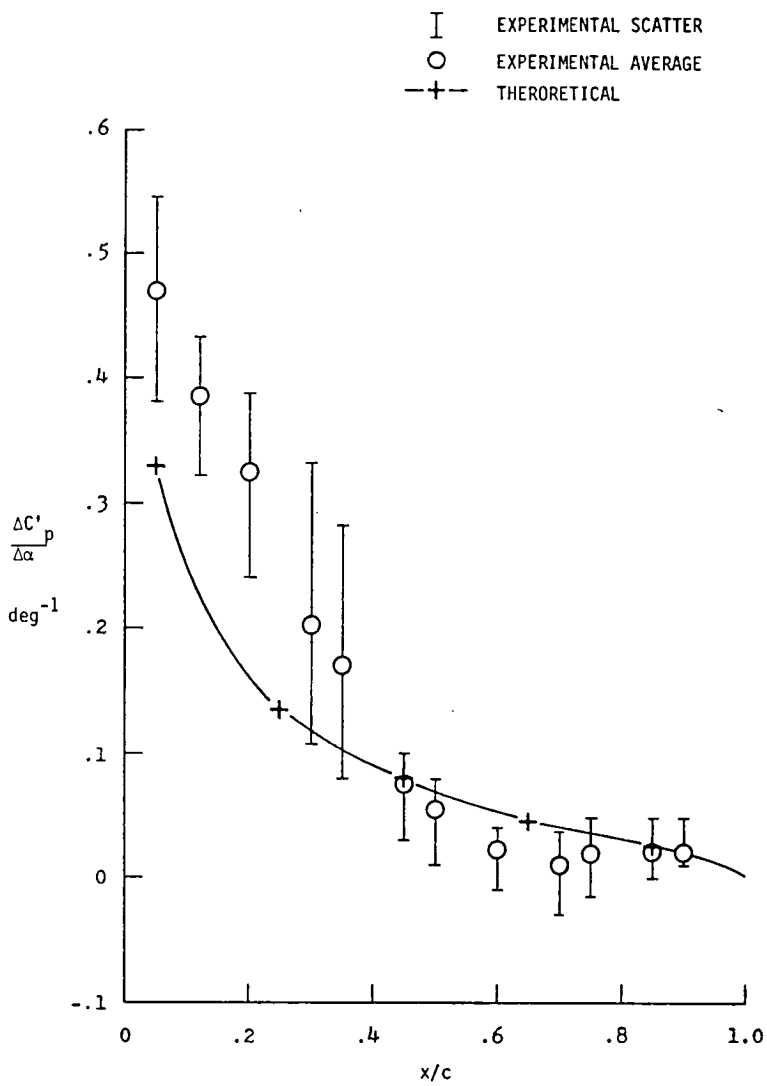

(i) $\eta = 0.92$

Figure 5. - Concluded.

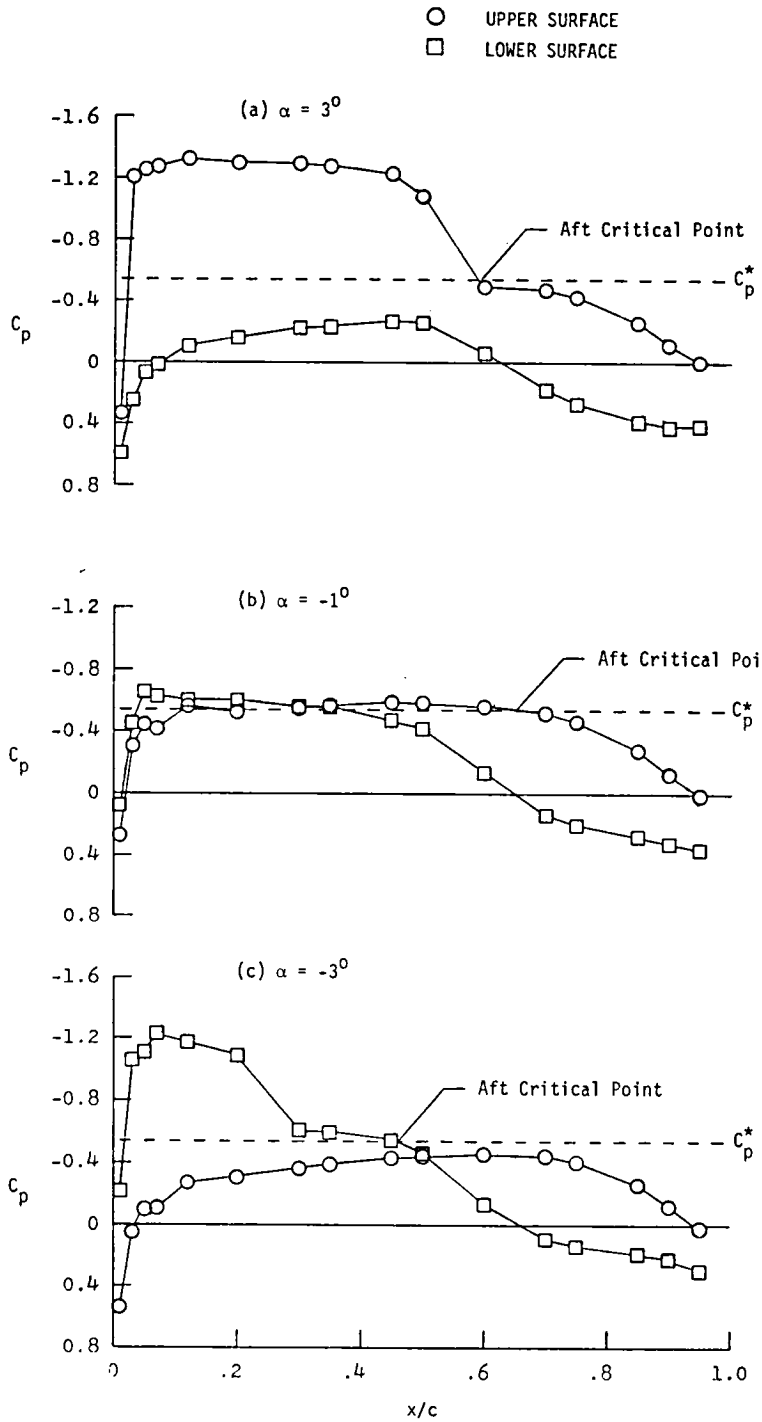

Figure 6. - Experimental surface steady-pressure coefficients at semispan station $\eta = 0.51$. Aft critical points defined by the downstream termination of critical flow on the surface.

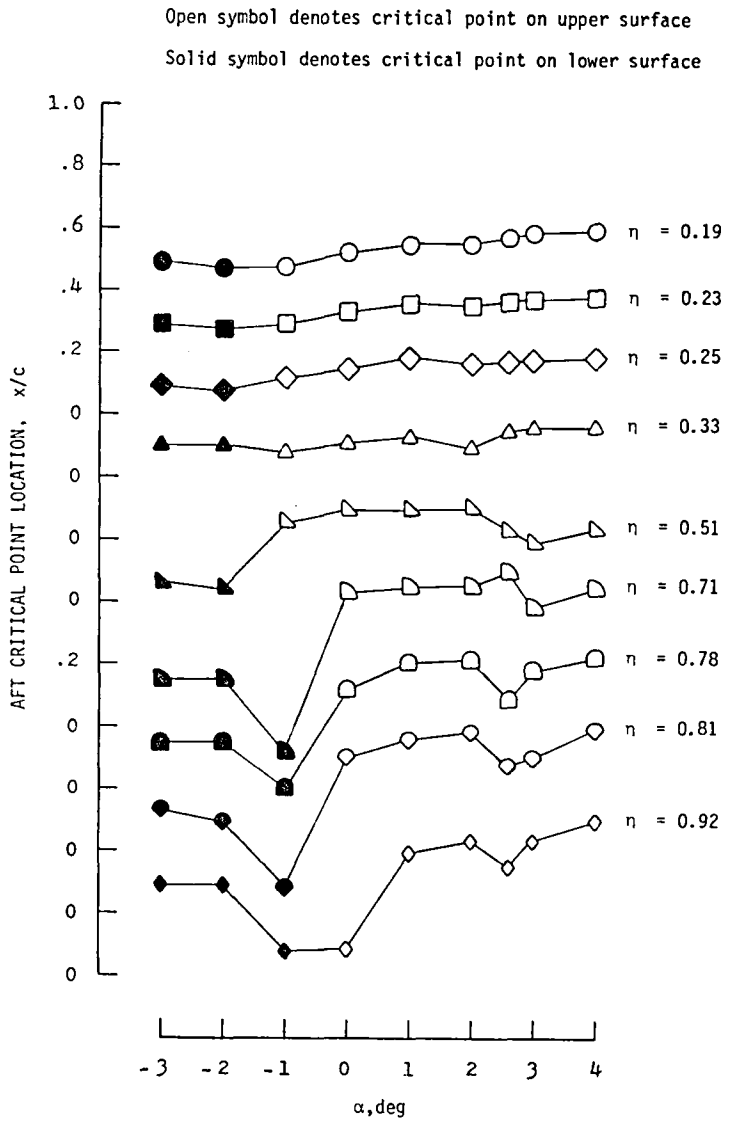

Figure 7. - Effect of angle of attack on aft critical point locations.

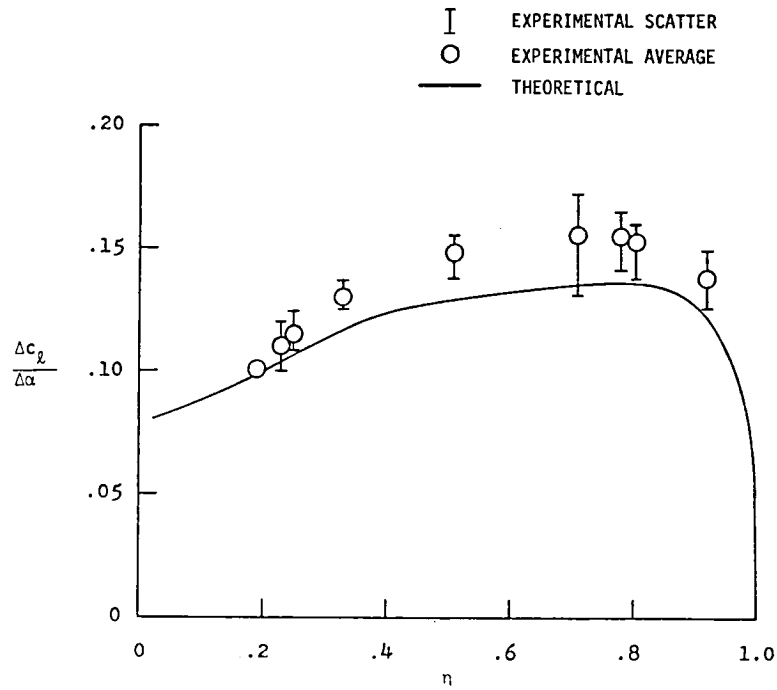

(a) Incremental section lift coefficient.

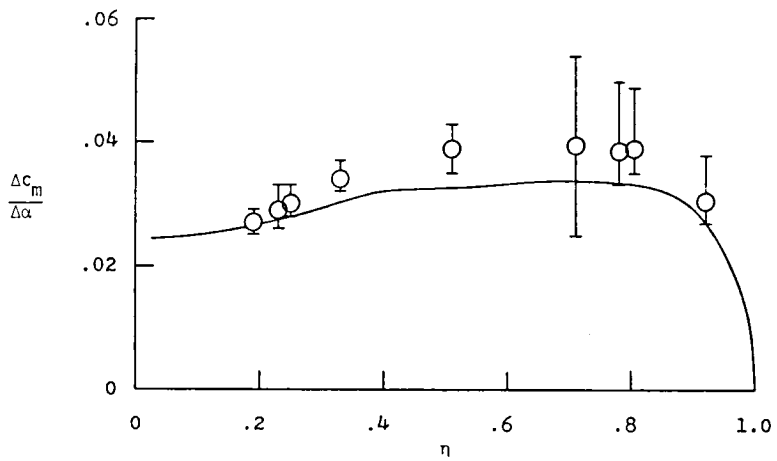

(b) Incremental section pitching-moment coefficient.

Figure 8. - Spanwise lift and moment distributions per incremental angle of attack.

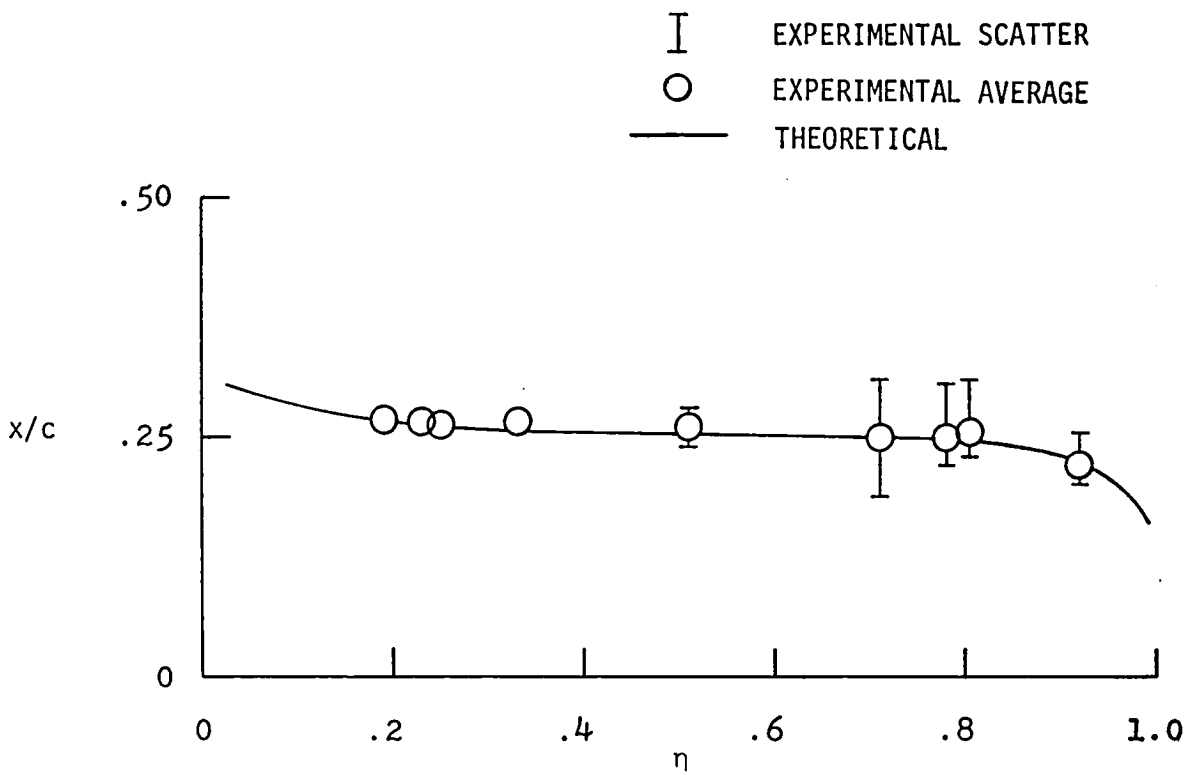

Figure 9. - Spanwise distribution of local aerodynamic center locations.

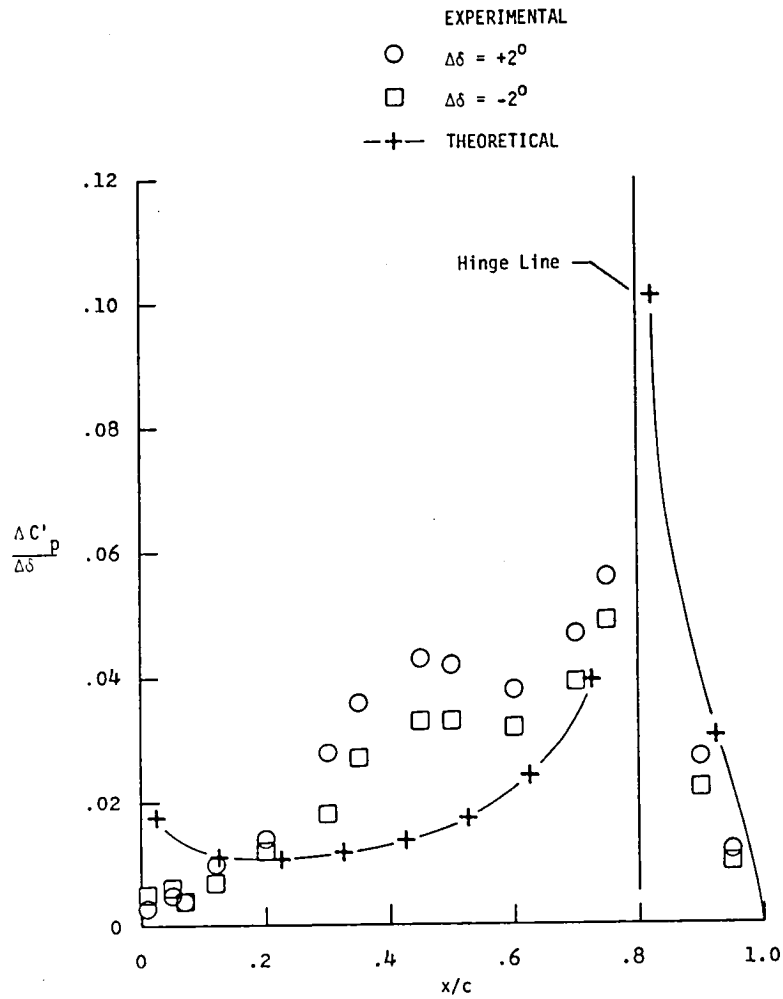

(a) $\Delta\delta = +2^{o}$ and -2^{o}

Figure 10. - Chordwise incremental lifting-surface steady-pressure distribution per incremental inboard control-surface deflection at semispan station $\eta = 0.19$. ($\alpha = 2.05^{o}$)

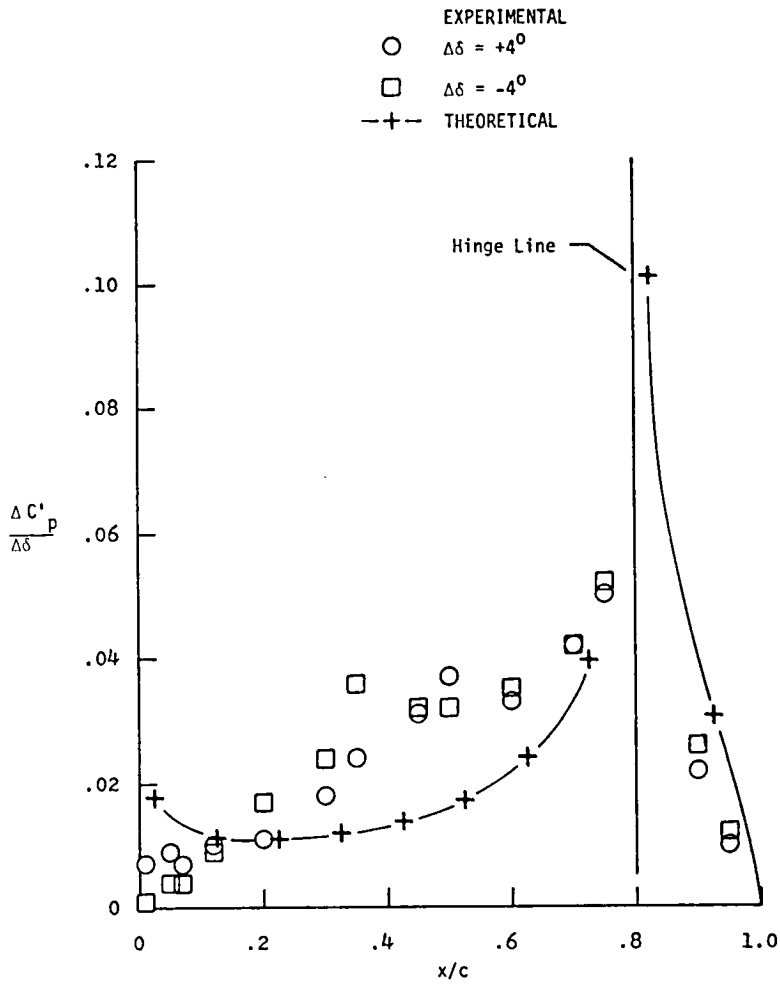

(b) $\Delta\delta = +4^{\circ}$ and -4°

Figure 10. - Continued.

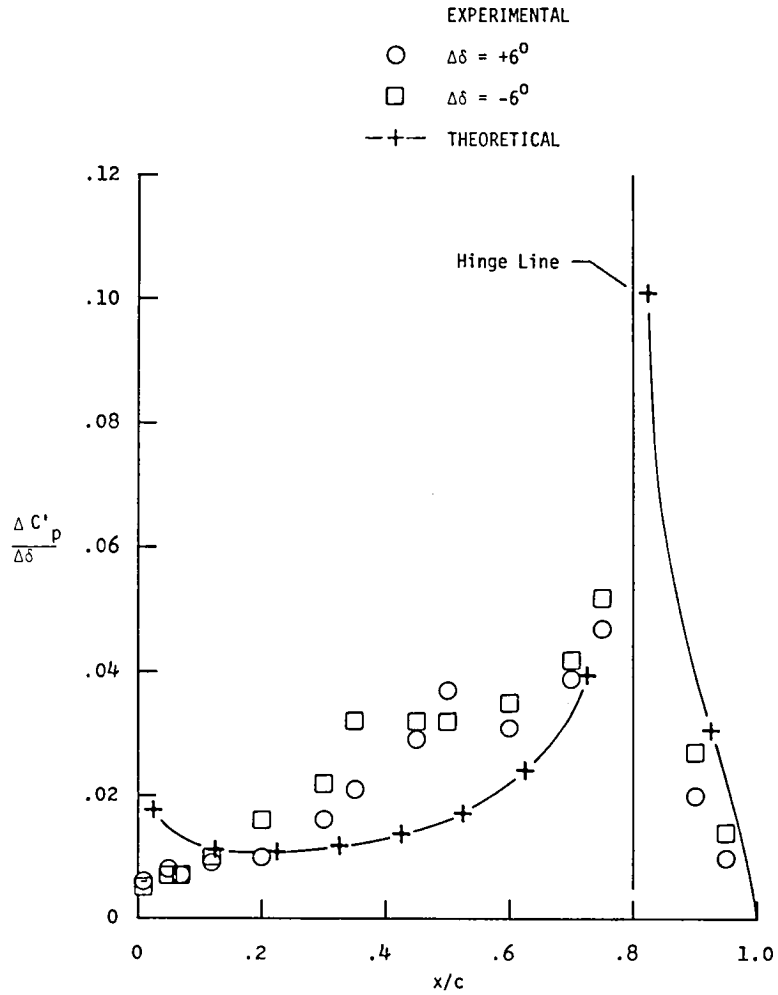

(c) $\Delta\delta = +6^{o}$ and -6^{o}

Figure 10. - Concluded.

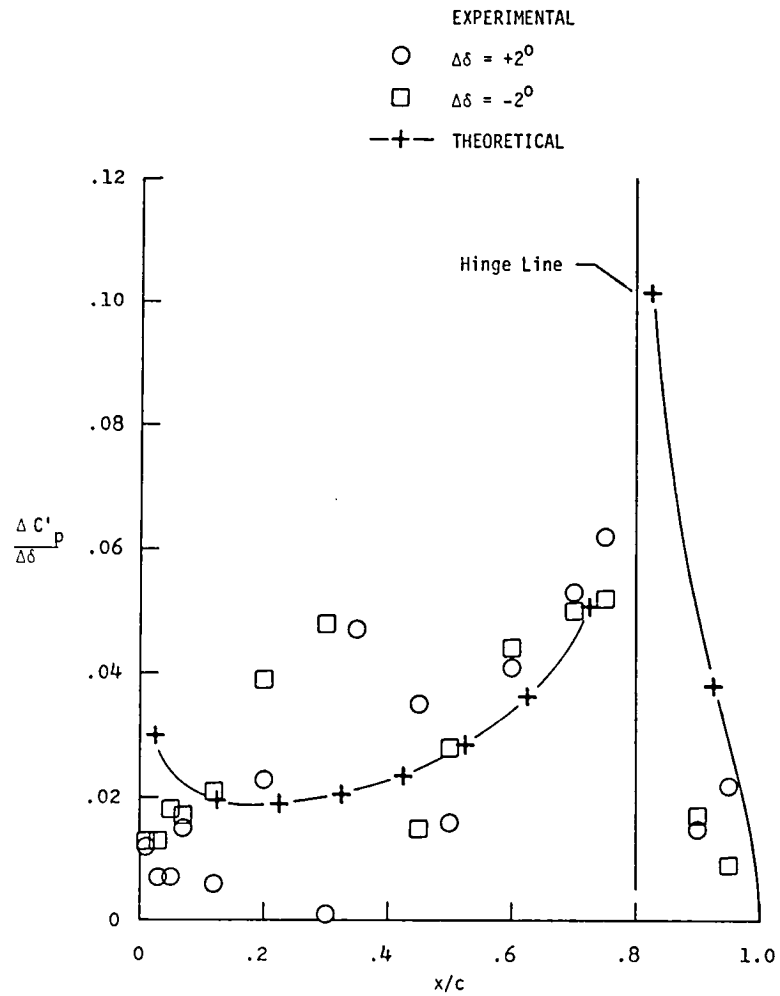

(a) $\Delta\delta = +2^{o}$ and -2^{o}

Figure 11. - Chordwise incremental lifting-surface steady-pressure distribution per incremental outboard control-surface deflection at semispan station $\eta = 071$. ($\alpha = 2.05^{o}$)

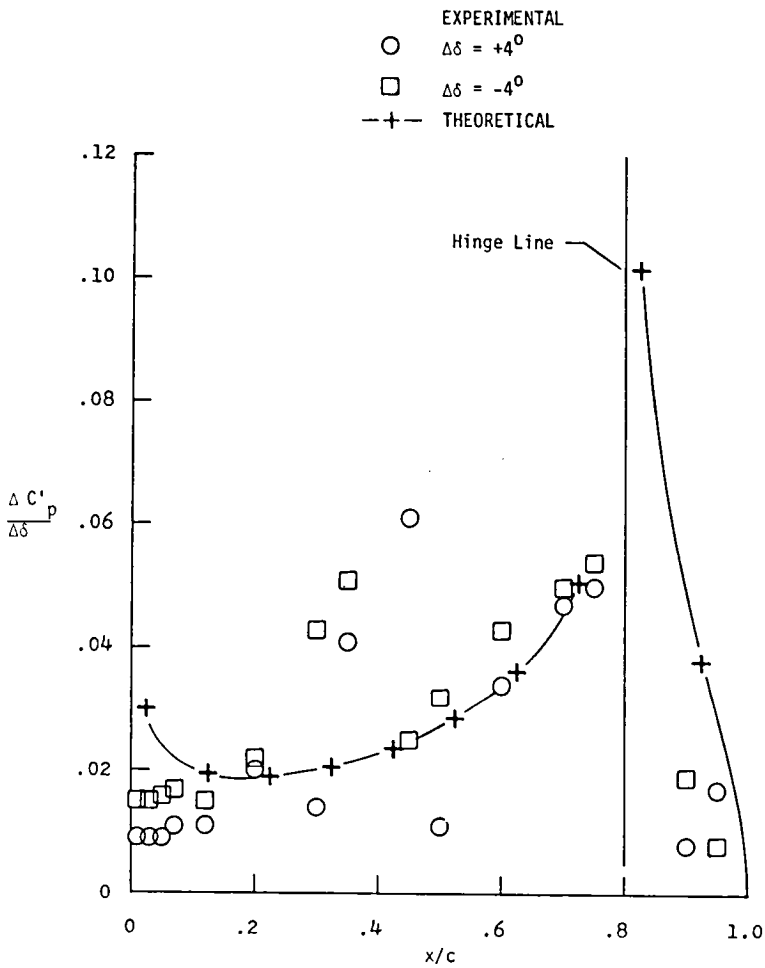

(b) $\Delta\delta = +4^{o}$ and -4^{o}

Figure 11. - Continued.

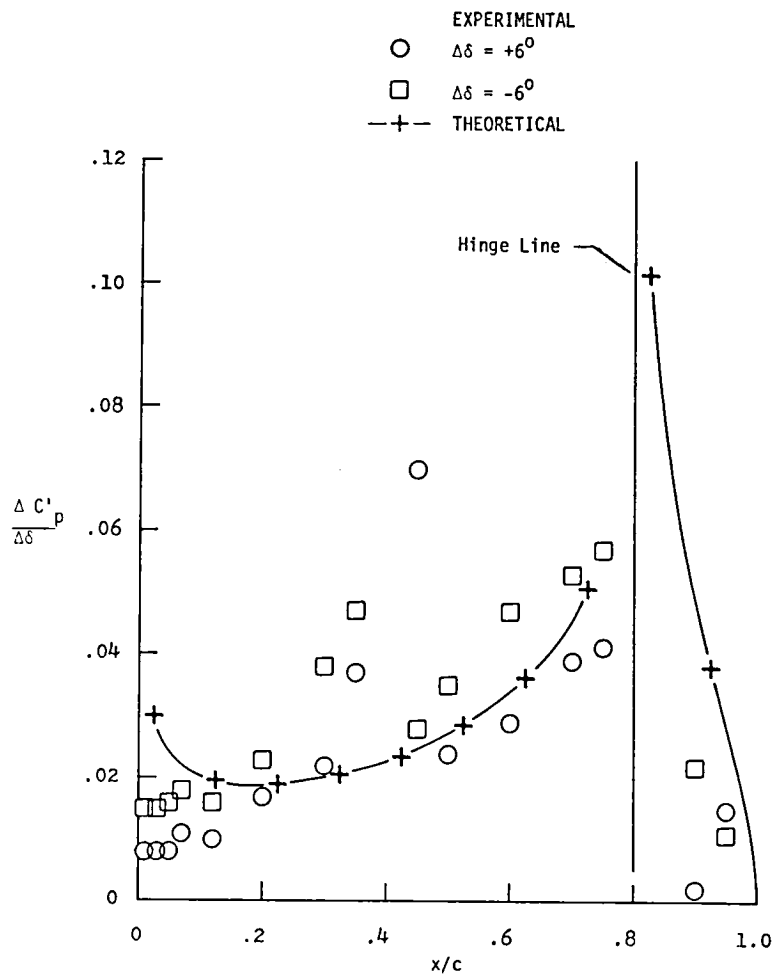

(c) $\Delta\delta = +6^{\circ}$ and -6°

Figure 11. - Concluded.

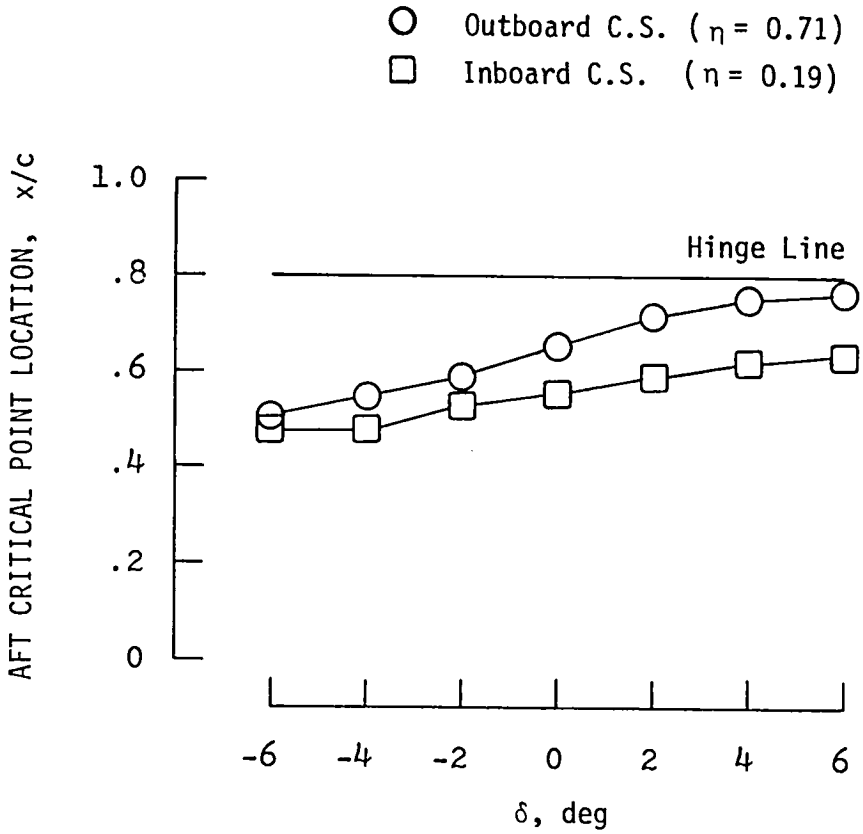

Figure 12. - Effect of control-surface deflection on aft critical point locations. ($\alpha = 2.05^{o}$)

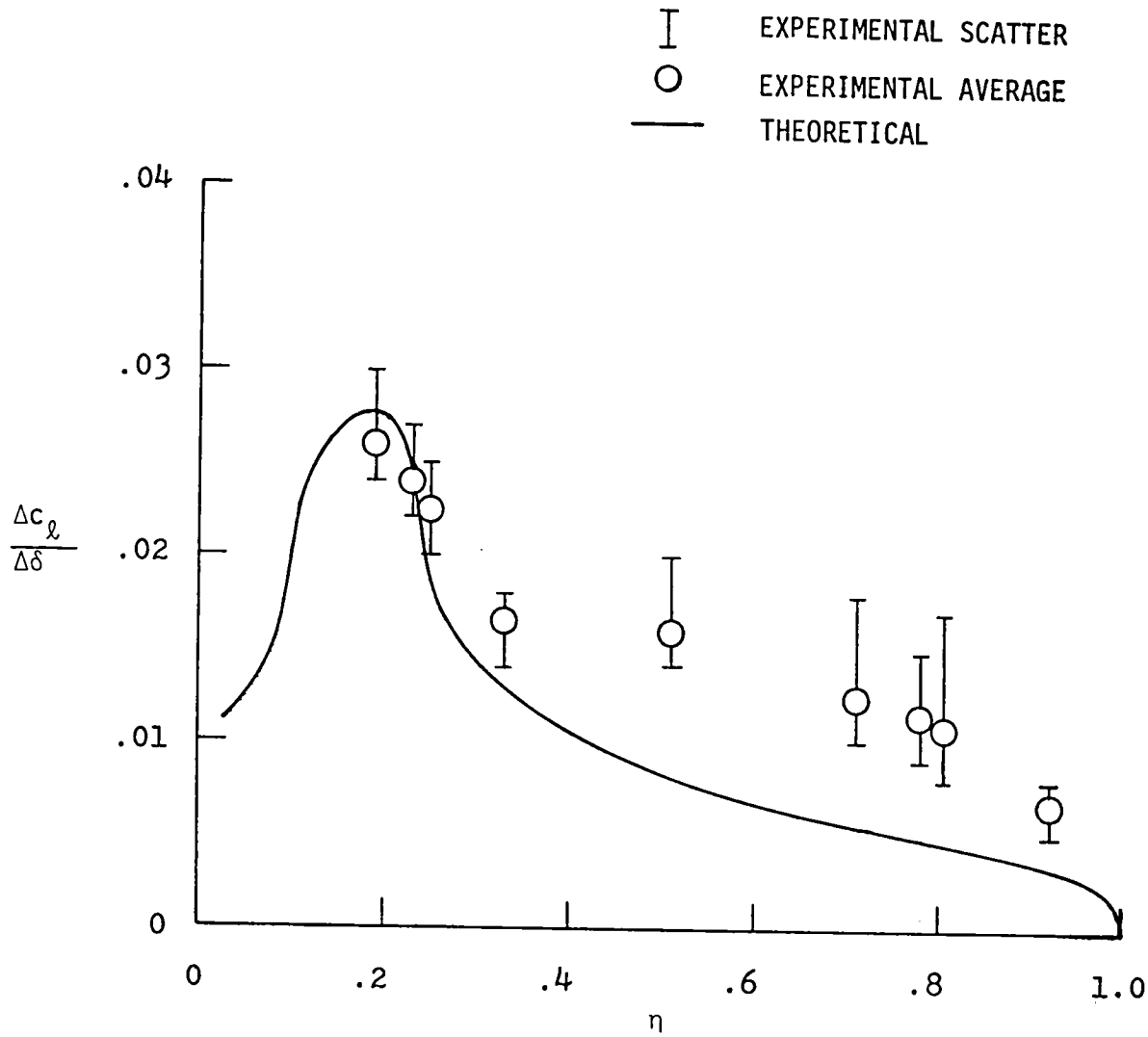

(a) Inboard Control Surface.

Figure 13. - Spanwise lift distributions for incremental control-surface deflections.

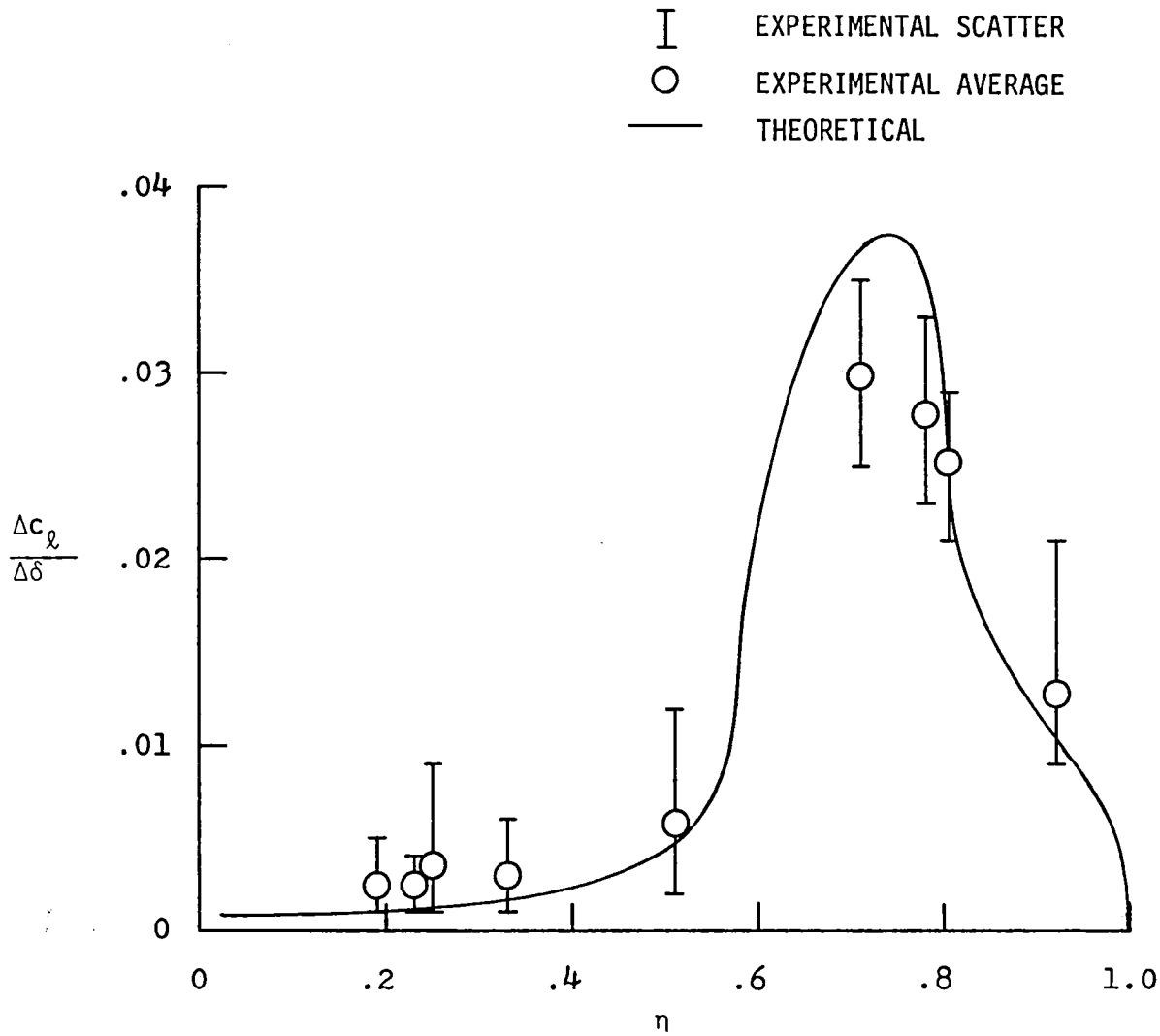

(b) Outboard Control Surface.

Figure 13. - Concluded.

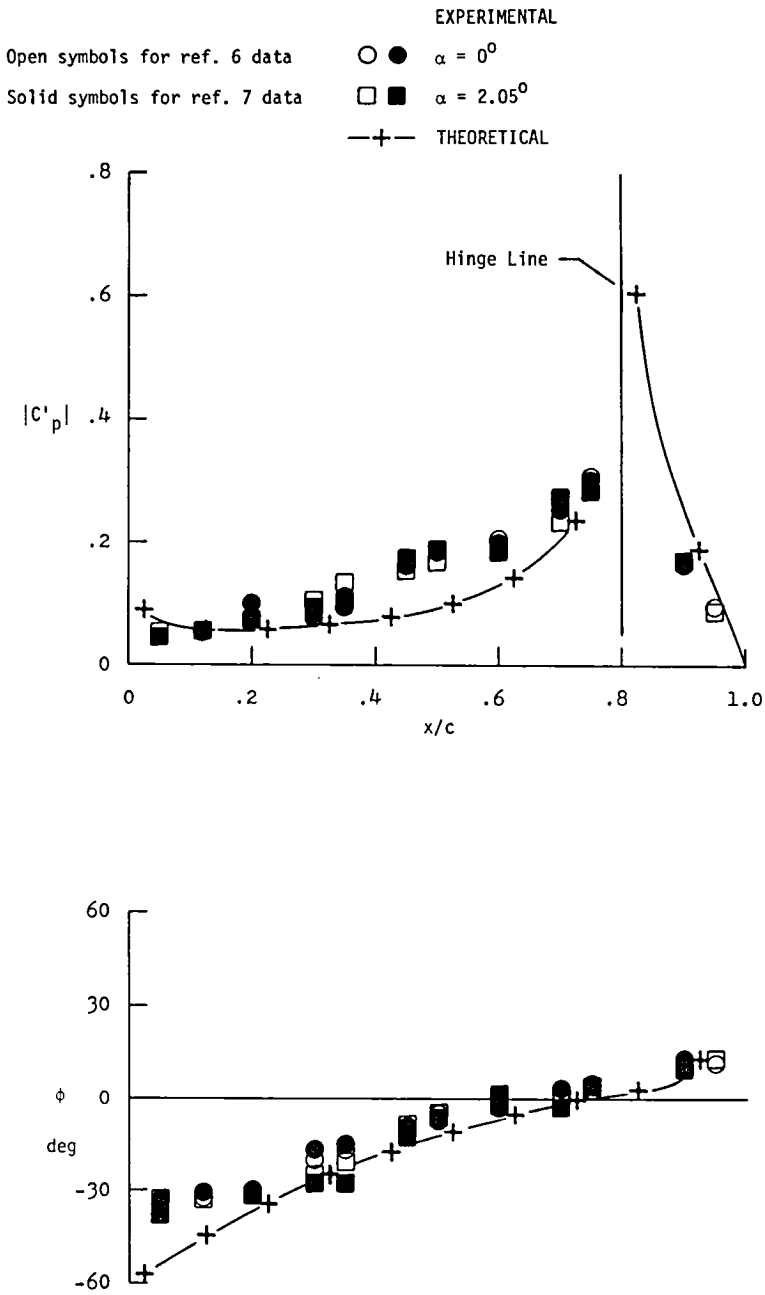

(a) k = 0.105 (f = 5 Hz)

Figure 14. - Magnitude and phase angle of chordwise lifting-surface unsteady pressure distribution at semispan station η= 0.18, due to oscillating inboard control surface. ($\delta = \pm 6^{o}$)

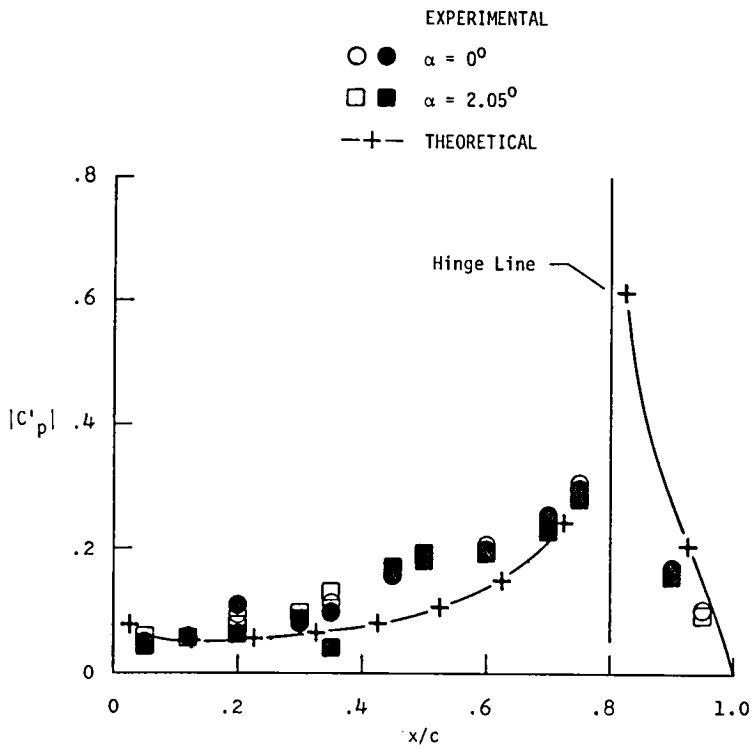

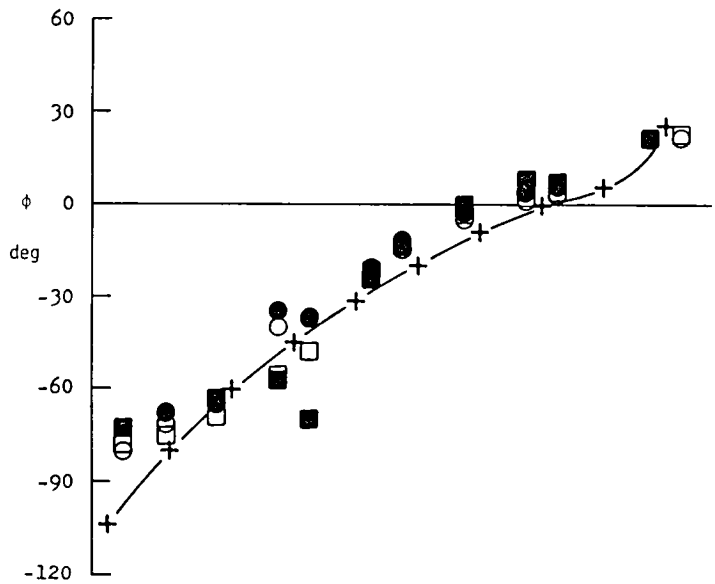

(b) k = 0.210 (f = 10 Hz)

Figure 14. - Continued.

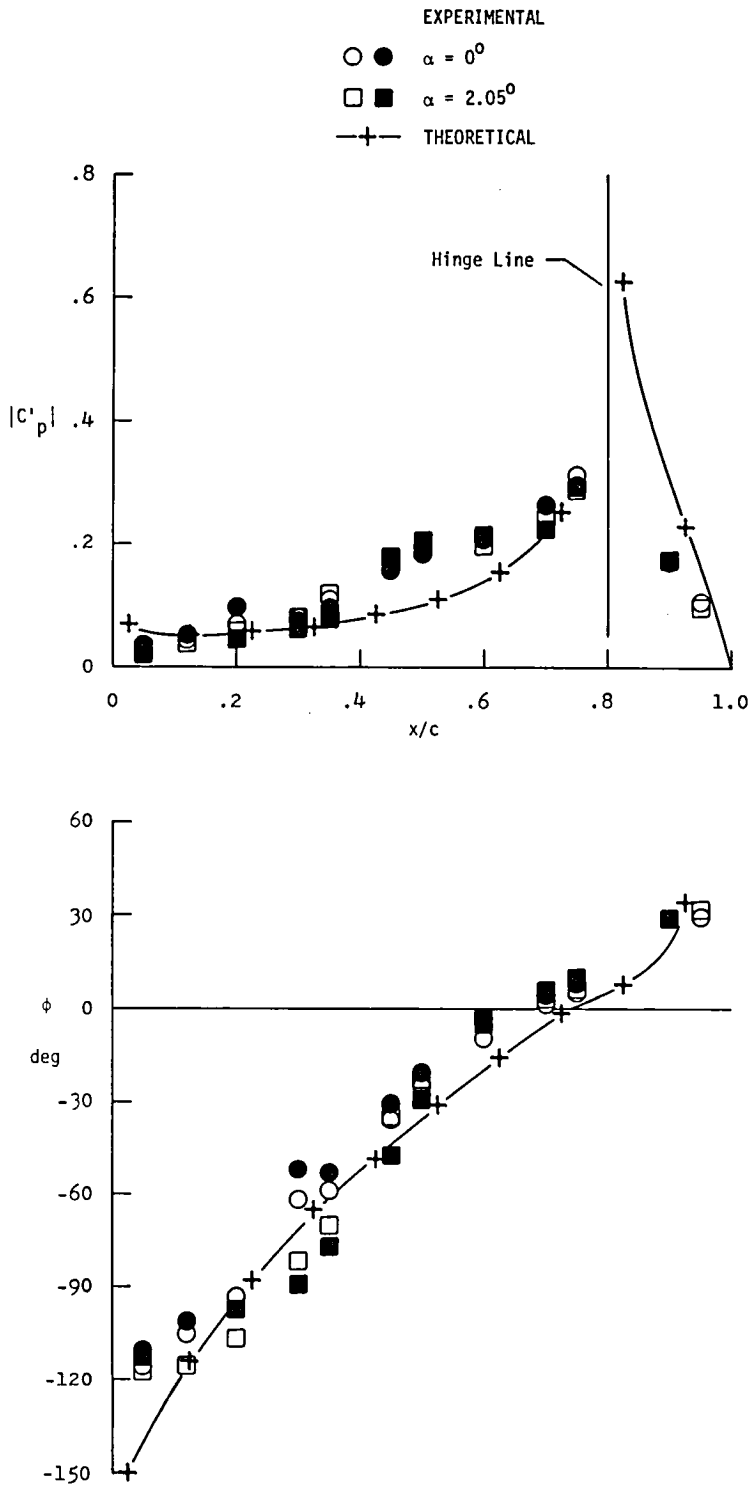

(c) k = 0.315 (f = 15 Hz)

Figure 14. - Concluded.

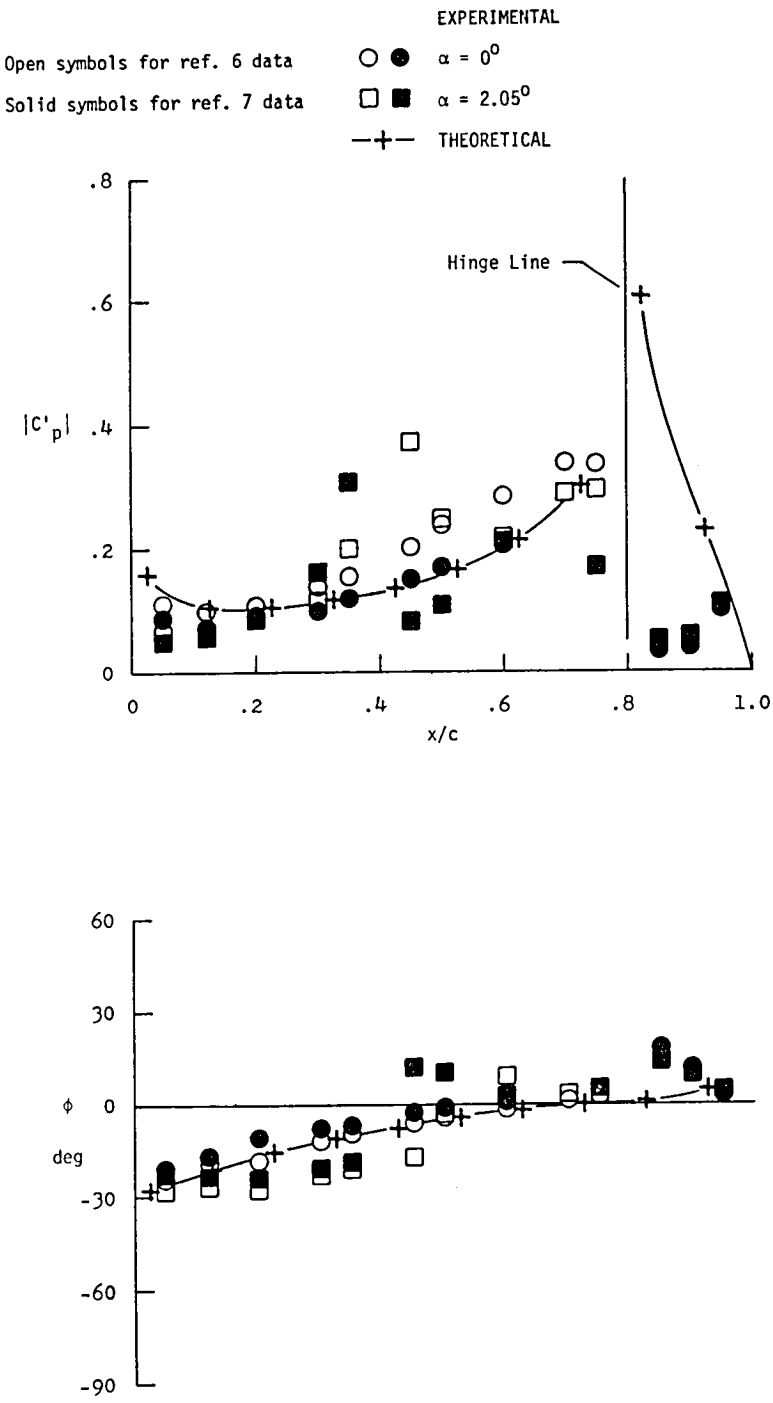

(a) k = 0.105 (f = 5 Hz)

Figure 15. Magnitude and phase angle of chordwise lifting-surface unsteady pressure distribution at semispan station η= 0.71, due to oscillating outboard control surface. ($\delta = \pm 6^{o}$)

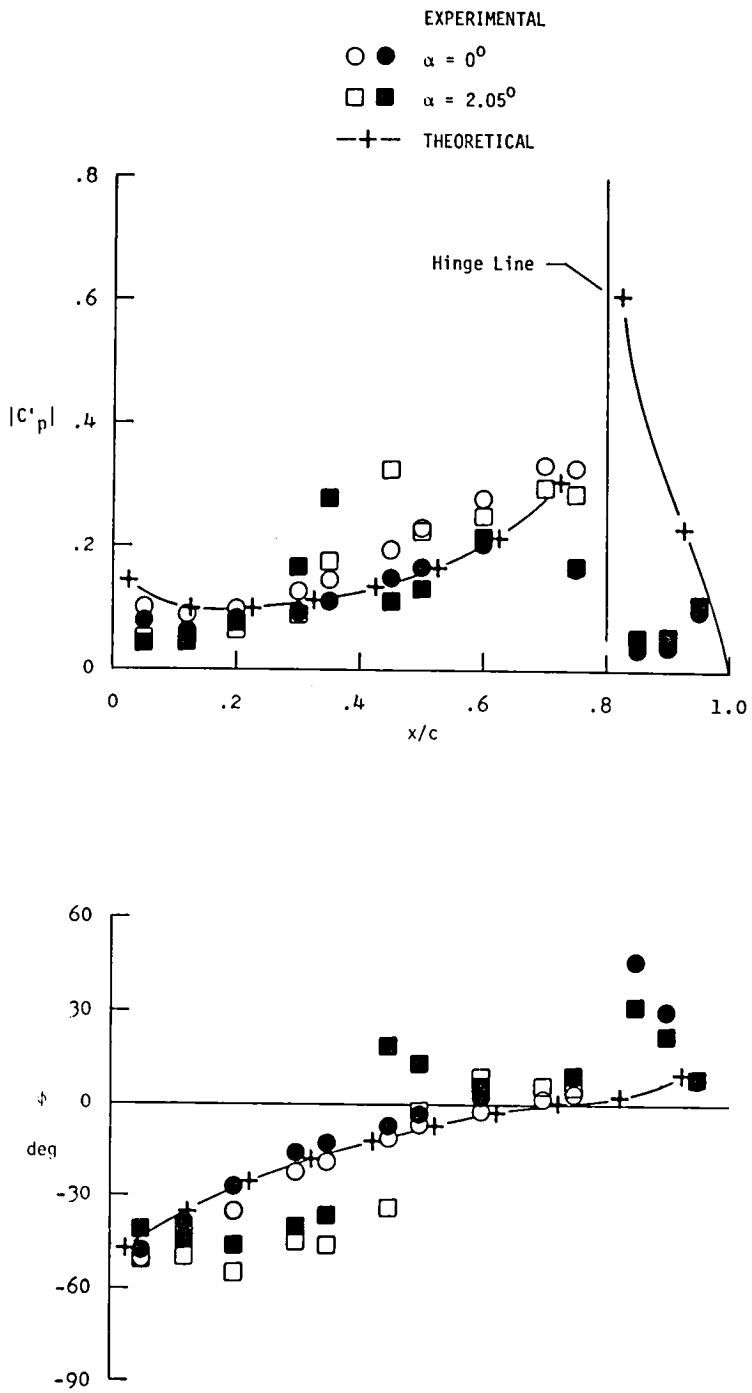

(b) k = 0.210 (f = 10 Hz)

Figure 15. - Continued.

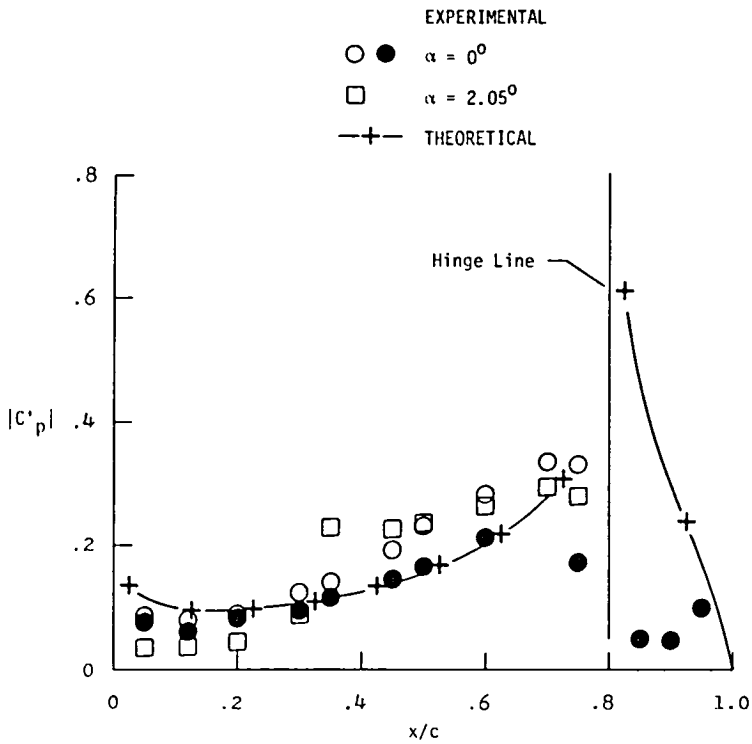

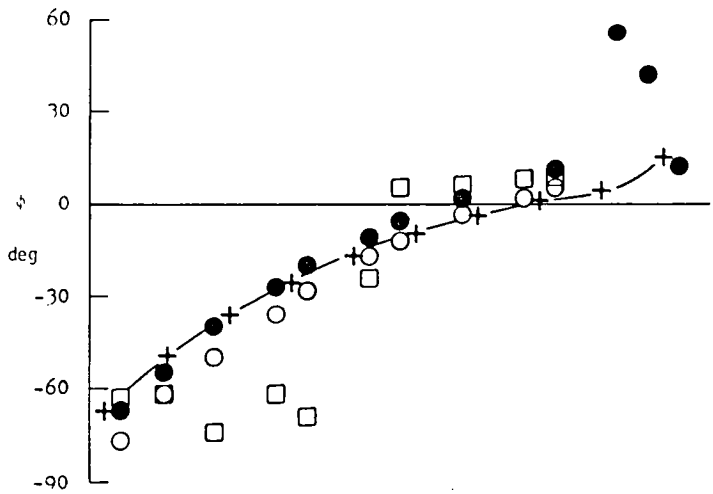

(c) k = 0.315 (f = 15 Hz)

Figure 15. - Concluded.

1. Report No.	2. Government Accession No.	3. Recipient's Catalog No.
NASA TM 84589		

4. Title and Subtitle	5. Report Date
COMPARISON OF ANALYTICAL AND EXPERIMENTAL STEADY- AND UNSTEADY-PRESSURE DISTRIBUTIONS AT MACH NUMBER 0.78 FOR A HIGH-ASPECT-RATIO SUPERCRITICAL WING MODEL WITH OSCILLATING CONTROL SURFACES	January 1983
	6. Performing Organization Code 505-33-53-13
7. Author(s) William E. McCain	8. Performing Organization Report No.
	10. Work Unit No.
9. Performing Organization Name and Address National Aeronautics and Space Administration Langley Research Center Hampton, VA 23665	11. Contract or Grant No.
	13. Type of Report and Period Covered Technical Memorandum
12. Sponsoring Agency Name and Address National Aeronautics and Space Administration Washington, DC 20546	14. Sponsoring Agency Code

15. Supplementary Notes

16. Abstract

This paper presents a comparative study of the unsteady aerodynamic lifting-surface theory, known as the Doublet Lattice method, with experimental steady- and unsteady-pressure measurements of a high-aspect-ratio supercritical wing model at a Mach number of 0.78. The steady-pressure data comparisons were made for incremental changes in angle of attack and control-surface deflection. The unsteady-pressure data comparisons were made at set angle of attack positions with oscillating control-surface deflections. Comparative results showed significant viscous and transonic effects in the experimental aerodynamics which cannot be predicted by the Doublet Lattice method. This study should assist development of empirical correction methods that may be applied to improve Doublet Lattice calculations of lifting-surface aerodynamics.

17. Key Words (Suggested by Author(s))	18. Distribution Statement
Doublet Lattice, oscillating control surface transonic steady- and unsteady-pressures	~~FEDD Distribution~~ Subject Category - 02

19. Security Classif. (of this report)	20. Security Classif. (of this page)	21. No. of Pages	22. Price
Unclassified	Unclassified	55	

Available: NASA's Industrial Applications Centers